International Journal of Material Forming (2024) 17:53
https://doi.org/10.1007/s12289-024-01855-7

REVIEW

Evaluating residual stresses in metal additive manufacturing: a comprehensive review of detection methods, impact, and mitigation strategies

Mumtaz Rizwee[1] · **Deepak Kumar**[1]

Received: 2 March 2024 / Accepted: 3 September 2024

Abstract

The metal additive manufacturing (MAM) process has most employed methods to build complex geometry and light-weight 3-dimensional (3-D) parts directly from a computerized solid model. Distortion of the printed part is a highly significant concern within the MAM process. This issue is because of the heating and cooling effect of printing process that could accumulate residual stress (RS) during part building up. The aim of the literature work is to present various methodologies for measuring RS in MAM components and to furnish a brief summary of recent developments in the domain. These details aid scholars in the discernment of suitable techniques, namely destructive, semi-destructive, or non-destructive, contingent on their particular applications and the accessibility of these methods. Moreover, it facilitates the explication of their formation mechanisms, effectiveness of process parameters, prediction, and control techniques. The effect of RS on the mechanical characteristics of printed parts is analyzed and presented. Additionally, common defects incorporated into RS are discussed. Moreover, this review article discusses about the future challenges and opportunities in the RS analysis of MAM parts.

Highlights

●Different technique of residual stress measurement in additive manufacturing process.
●Influence of process parameter on residual stress.
Scanning speed, layer height, laser power, laser energy density etc.
●Impact of residual stress on mechanical properties.
●Common defect due to residual stress.
Delamination, parts cracking, separation from support, grain boundary cracking etc.
●Impact of in-process and post-process techniques in residual stress modification.
Shot peening, heat treatment, hot isotatic pressing, laser shock peening etc.

Keywords MAM · RS · Mechanical properties · Distortion · RS control method

Introduction

Residual stresses refer to the internal stresses that remain in a manufactured component even without the presence of external forces and thermal gradients, and are self-equilibrating in nature. These stresses are caused by mismatches in the geometry of components from various regions and phases within a part, as well as regional disparities in elastic moduli, thermal properties, and mechanical attributes, and solid-state phase transition shown in Fig. 1 [1]. The presence of RS can result in a multitude of adverse effects on

✉ Deepak Kumar
deepak.me@nitjsr.ac.in

[1] Advanced Composite and Smart Material Laboratory, Department of Mechanical Engineering, National Institute of Technology Jamshedpur, Jharkhand 831014, India

Published online: 14 September 2024

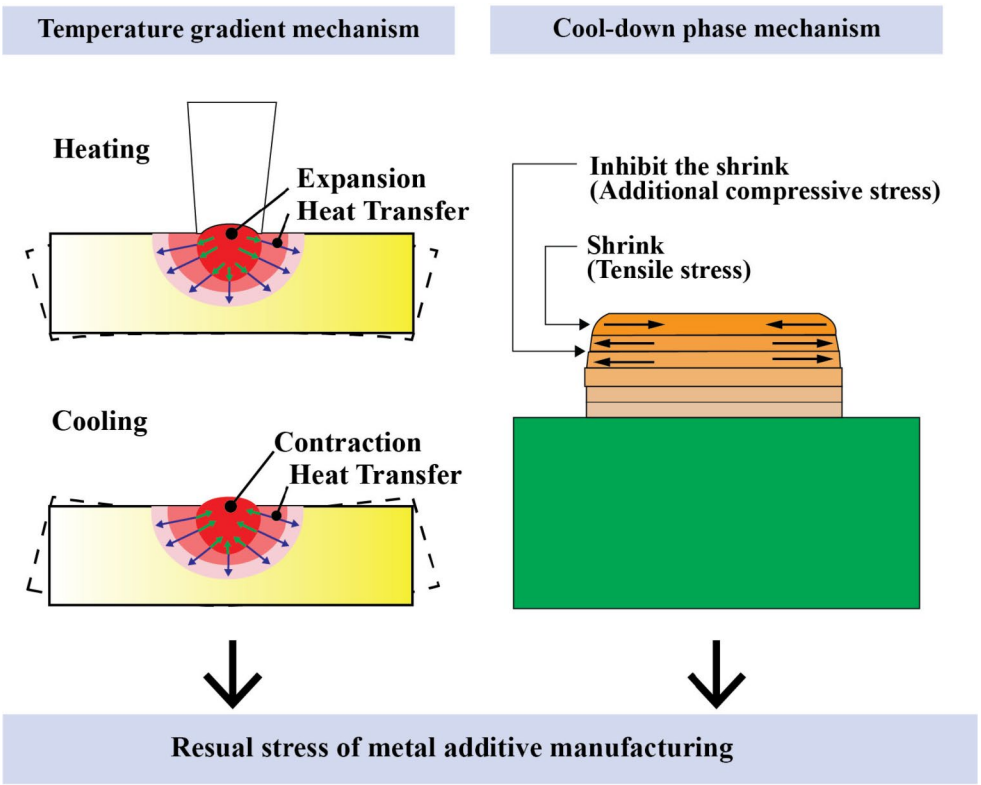

Fig. 1 Residual stress formation mechanism in MAM

the characteristics of a component, such as a lack of endurance against fatigue, consequential operational failure, diminished chemical resistance, reduced magnetization, decreased deformation resistance, and weakened static and dynamic strength [2]. In addition to leading to the formation of RS, service loading can cause uneven plastic deformation. The aforementioned stresses are present not solely in the end products, but also in the basic materials. There are four primary classifications for RS's origin [3], i.e., differential plastic flow, rapid cooling and heating rates, phase transformation accompanied by volume changes, and misfits induced by chemical factors.

The majority of MAM methodologies involve the utilization of a laser, plasma, or electron power source to induce rapid heating, which leads to liquefaction and subsequent solidification of the metal, whether it be in powder or wire form. The local structure and properties of components can be modified through repeated cycles of heating and cooling [4]. Due to the high freezing and heating rates, RS is produced, which can lead to deformation, cracking, and a reduction in the performance of additive manufacturing (AM) -produced materials. In addition, a direct consequence of RS is creating a pronounced anisotropic behaviour in these materials [3].

The RS are not independent occurrences; instead, they appear as complementary and opposing forces (tensile and compressive) or circumstances that arises compressive and tensile RS within a material. Understanding this duality is crucial in engineering and materials science because it can significantly influence the performance and integrity of components and structures. Compressive RS implies the internal forces or contractions experienced by a specimen in the inward direction. It may develop as a result of various manufacturing procedures, including heat treatment. It exhibits a tendency to impede crack propagation and has the potential to augment the material's resistance to fatigue and tensile loading. Alternatively, tensile RS induces outward forces or expansions within a specimen. It may manifest as a result of various procedures such as machining, surface grinding, or rapid cooling. The application of tensile RS has the potential to increase the part's susceptibility to the initiation and propagation of cracks, thereby affecting its structural integrity. The presence of both compressive and tensile residual stresses in a material means that they are, in essence, a paired phenomenon. These pairs of stresses must be carefully managed and balanced so that attempt should be to have compressive residual stress at the surface and tensile within the volume to ensure the safe and reliable performance of components and structures.

The Temperature gradient mechanism (TGM), shown in Fig. 2, can explain the origins of RS in MAM. The power source induces local elastoplastic deformations (designated by ε_{pl}, ε_{el}, and σ_{yield}) and additional tensile tension in the irradiated zone upon heating. Thermal contraction induces diminution and the formation of tensile and compressive RS regions (top and bottom layers, respectively) during the

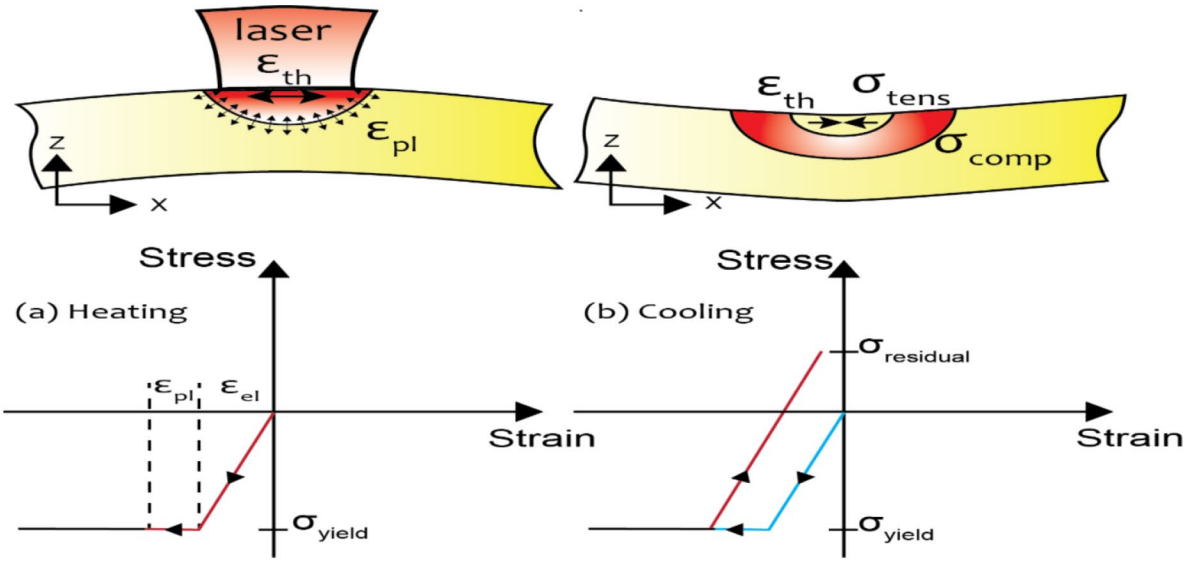

Fig. 2 (**a**) Heating and (**b**) cooling effect on stress/strain in the irradiated zone

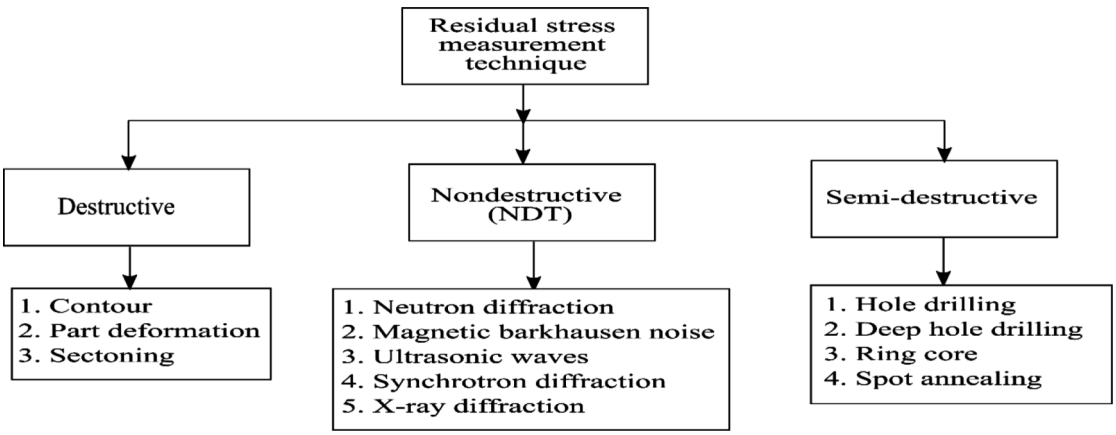

Fig. 3 Residual Stress measurement techniques

cooling of the molten top layers [4, 5]. The temperature in nearby areas where the heating source (laser/electron beam/plasma) interacts with the powder undergoes rapid escalation. However, the expansion of the hot material region is constrained by the cooler regions that surround it. The imposition of this limitation results in the generation of compressive stress within the region of the material that is at an elevated temperature. The cooling and contraction of the hot region are constrained by the surrounding regions, resulting in the development of permanent tensile RS in the surface of the fabricated part (Figs. 1 and 2). Due to the complexity of the MAM process, the TGM model is merely a simplification of how RS is generated [5]. The formation and intensity of RS are influenced by a multitude of factors, such as the material's properties (e.g., grain size, heat capacity, porosity and phase composition), the specimen's geometry, the necessary support structure, and the printing parameters (e.g., laser or electron beam power, pre-heating method, scanning strategies and speed, and layer height) [3, 5]. In addition, the estimation of RS is influenced by various factors, including elastic constants, nonlinearity resulting from texture, stress gradient with depth, micro stresses caused by plastic deformation, and grain interactions [6].

Non-destructive, semi-destructive, and destructive measurement techniques are the three fundamental RS measurement categories. Several types of each category are shown in Fig. 3. The digital photographs of different RS measurement setups are depicted in Fig. 4. In non-destructive methods (NDT), the crystal lattice strain is measured. Then, the corresponding values of RS are calculated using elastic constants under the assumption that the crystal lattice deforms linearly elastically [7, 8]. NDT techniques have a variety of advantages and drawbacks, summarized in Table 1.

Destructive techniques include eliminating certain pieces of a sample to alleviate RS. The resulting deformations and their associated stresses are then formed. These techniques

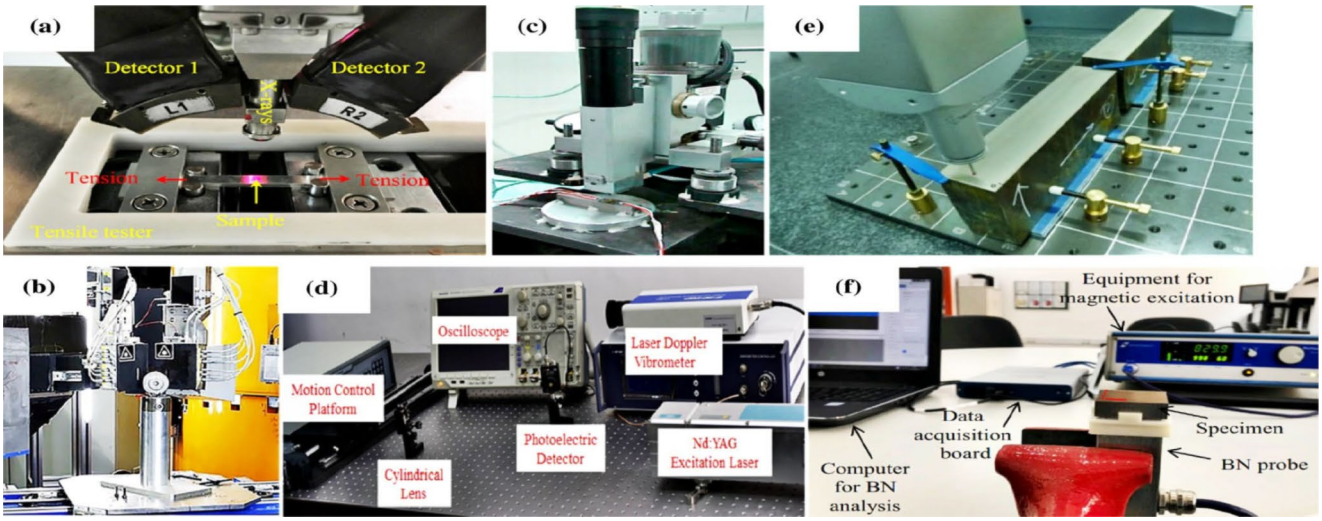

Fig. 4 RS measurement setup: (**a**) XRD stress measurement system [10], (**b**) Neutron diffractometer [11], (**c**) MTS 3000-hole drilling system [12], (**d**) Ultrasonic system [13], (**e**) Contour RS system [14], (**f**) Barkhausen Noise evaluation [15]. Reproduced with permission from Elsevier

often demand Finite Element Method (FEM) tools to evaluate deformation behaviour and determine RS values [9]. As a middle scenario, fewer property changes are brought about by semi-destructive procedures than by destructive ones. The most popular of them is hole drilling (HD). This technique is predicated upon the fundamental idea that the introduction of a tiny aperture into a material serves to alleviate a portion of the RS present in the immediate area of such aperture. The application of stress relief induces a localized deformation inside the material, and the subsequent strain is determined as the hole is progressively deeper. The strain measurements are often obtained by observing changes in strain components, particularly normal strains, as a function of depth. The alterations in strain are correlated with the variations in residual stresses, and these measurements are used in future computations. The contour approach is one of the destructive methods that facilitates the evaluation of a two-dimensional RS map on a specific plane of interest. The contour approach offers enhanced spatial resolution, but the sectioning technique is characterized by its ease of use, requiring minimal computations. The contour approach is founded upon the principle of dividing a material or component into slender parts, sometimes referred to as slices, and quantifying the deformation experienced by each segment upon its separation from the adjacent material. The presence of RS inside the material induces deformations in the sliced parts, resulting in either an opening or closing effect upon removal. These deformations are then used to deduce the distribution of RS. The deformation data that has been gathered is analyzed in order to determine the distribution of RS inside the material. Computational approaches, such as the FEM or analytical models, are often used for this purpose. The contour plots depict the distribution of RS that has been determined by calculation. These plots visually represent the varying stress levels at various spatial positions inside the material. The contour technique is extensively used across several sectors, such as aerospace, automotive, and manufacturing, for the purpose of evaluating the RS condition in crucial components. These components may include weld joints, turbine blades, forged materials, quenched and impacted thick plates, as well as structural materials. Table 1 summarizes the comparative analysis among the different categories of RS measurement regarding advantages and drawbacks. Because of their accessibility, the abundance of recognized standards (ASTM, ISO, etc.), and ease of measurement, HD, Ultrasonic wave, and X-ray diffraction (XRD) are now the most used methods for RS measurement in MAM [3].

Considerable research about RS in MAM has revealed several significant correlations. However, there is a lack of literature reviews in this field. Although review papers play a crucial role in elucidating the RS of MAM, there is currently a dearth of a comprehensive and systematic literature that encompasses the current state of the formation mechanism, parameter dependence, prediction, and adjustment approach of RS in MAM. Additionally, this review has focused on LPBF techniques due to its widespread use in producing high-precision, auxetic behaviour [16], complex metal components, light weight components, which aligns closely with the objectives of this research. This literature work aims to address the lack of comprehensive information on RS studies in MAM. It aims to systematically summarize the significant findings in this field, including measurement and characterization techniques, formation mechanisms, printing parameter dependencies, defect incorporation,

Table 1 Comparative analysis among the residual stress measurement techniques

References	Method	Advantage	Limitation
[17, 18]	X-ray diffraction	Suitable for ductile material. Applicable for a wider range of materials. Measured macro and micro level RS. Non-destructive method	Limited depth of measurement. Surface damage. Suitable for small components. High-cost technique.
[19]	Hole drilling	Fast and more convenient to use. Suitable for a wider range of materials. Low-cost method. Specimen damage is often tolerable or repairable	Strain sensitivity and resolution are limited. Semi-destructive method. Data analysis required. Error sources.
[20–22]	Neutron diffraction	Determine macro and micro level RS. Larger penetration depth and high spatial resolution. Evaluate 3D map, non-destructive method More suitable for high average atomic number alloy	Data analysis required. Required specialist facility. High-cost technique.
[23, 24]	Magnetic Barkhausen noise	Fast and efficient Sensitive to microstructure effect Non-destructive method High sensitivity and non-contact measurement	Suitable for ferromagnetic materials. Interpretation of results required. Sensitivity to environmental noise.
[25–28]	Ultrasonic waves	Quick and low-cost method Measured interior RS, non-destructive method Free from radiation hazards Routine inspection of large components (steam turbine disks)	Limited spatial resolution. Required bulk measurements over whole volume.
[29–35]	Sectioning	More economical and appropriate for a wider range of materials. Hand-held system and easier to apply. Extensively used for carbon steel, aluminium, and stainless-steel sections.	Destructive method, time-consuming. Limited strain resolution. Sample size limitation and FEA required. Limited depth of measurement.
[36, 37]	Contour	Appropriate for a wider range of materials. Applicable for large components. Provide high-resolution 2D map Provide higher spatial resolution.	Destructive method. Required data interpretation. Finite element analysis (FEA) required.
[38–41, 3]	Deep hole drilling	Applicable for a wide range of materials. Suitable for a thick-sectioned specimen. Applicable to measure deep interior stresses.	Semi destructive method. Required data interpretation. Limited strain resolution and sensitivity.
[3]	Synchrotron Diffraction	Evaluate macro and micro level RS. Fast method. Enhanced penetration and resolution of X-rays. Suitable for depth profiling. Non-destructive method.	More expensive and time-consuming. Required specialist facility. Need for data analysis. Need for safety consideration.
[42, 43]	Ring core	Impart larger surface strain Easy to implement, low cost High accuracy	Semi destructive method. Create greater specimen damage. Less convenient to implement in practice.
[3]	Spot annealing	Cost-effective Minimal thermal damage Suitable for localized modification A fast and efficient method	Semi destructive method. Limited depth of modification. Limited modification area. High Precision Required.
[3]	Part deformation	Tailored properties Large modification area Cost-effective	Potential damage to the material. Limited applicability and time-consuming. Limited Precision.

mechanical properties degradation, and control techniques of RS in MAM.

This review paper first examines several techniques for measuring residual stress in the AM process, in order to build a basis for comprehending the progress made in analyzing RS in MAM. Then the literature examines the most recent research trends regarding the influence of process parameters on RS, the effect of RS on mechanical properties, RS analysis, and the impact of in-process and post-process techniques on RS modification. It emphasizes key findings and identifies gaps in the existing literature. Finally, this literature survey concludes by providing a concise overview of the important observations obtained from the review and puts up suggestions for furthering the area.

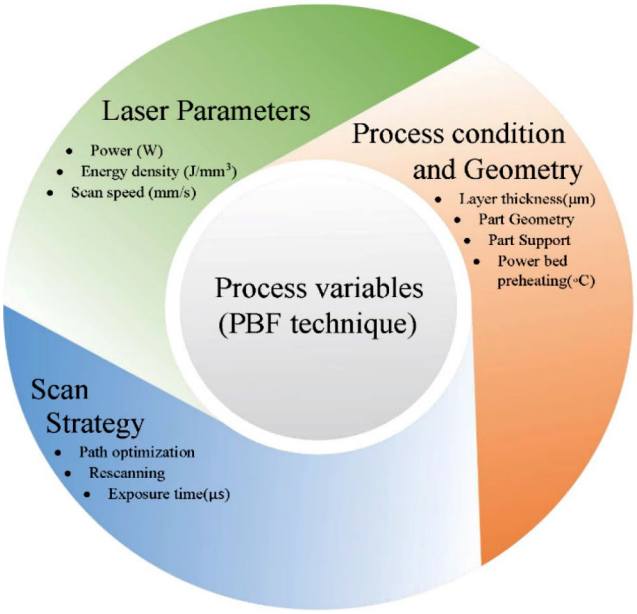

Fig. 5 Residual stress influencing process variable

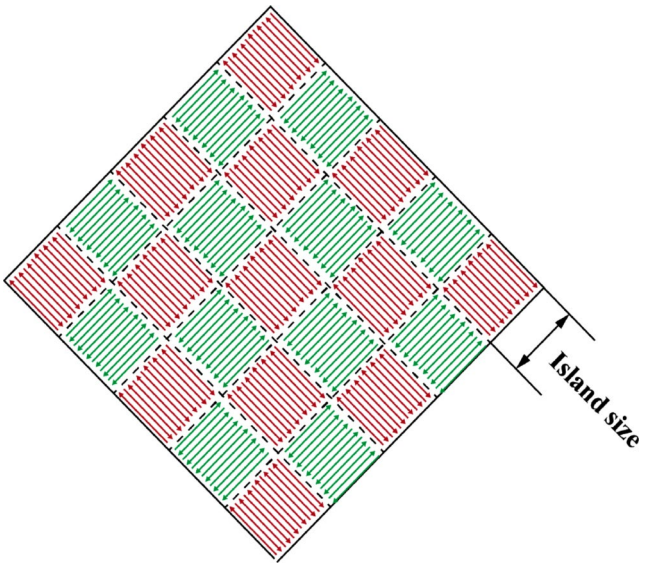

Fig. 6 Island Scanning Strategy

Impact of printing parameter on RS

Figure 5 compiles the process variables related to powder bed fusion (PBF) that impact RS. The fabrication process allows for adjusting beam/laser parameters and scan strategy. Conversely, certain process conditions, including factors such as part geometry and supports, are not readily amenable to in-situ modification. Among the variables, one of the crucial factors is the pre-heating of the powder bed, as it significantly reduces thermal gradients, minimizes part distortion, enhances dimensional accuracy and density, and improves mechanical characteristics [44, 45]. Maintaining an equilibrium between this parameter and other variables is imperative to prevent unfavourable outcomes such as excessive grain growth, recrystallization, and precipitation [46]. The mitigation of RS is significantly influenced by laser power and scan speed, irrespective of the material under consideration. Usually, elevated laser powers tend to generate increased RS levels due to the application of more incredible energy to the material, leading to a larger heat-affected zone (HAZ) and more pronounced thermal gradients. The phenomenon mentioned above has the potential to induce substantial deformation and modifications in the microstructural composition of the material, ultimately resulting in heightened RS. Determining the optimal laser power for minimizing RS is contingent upon the material under consideration and the intended final material properties, similar to the scanning speed. In certain instances, it may be imperative to utilize elevated laser powers to attain the intended degree of material modification, despite the accompanying escalation in RS [47–49]. Typically, the higher scanning speed reduces the amount of heat input into the build parts during the fabrication process because of very less heat exposure time. Less heat can lead to steeper thermal gradients, a smaller temperature differential between the melted and un-melted regions, and diminished size of the HAZ which can result in lower RS. The reduction in time available for thermal diffusion can impede the relaxation of the material and the formation of RS [47–52].

The scan strategy and its associated parameters (Fig. 5) have a multifaceted impact on stress, encompassing its distribution, direction, and magnitude [46]. Kruth et al. [4] investigated that utilizing the island scanning technique, which involves depositing material in a “chessboard” pattern shown in Fig. 6, would reduce distortion compared to alternative scanning strategies. The impact of island size on RS was investigated by Lu et al. [53], and a comparable pattern was detected in the findings of [54]. The research determined that the island size of 2×2 mm^2 yielded the lowest RS. However, the sample constructed with this island size also exhibited significant cracking. The optimal strategy was to consider an island with dimensions of 5×5 mm^2 due to its higher density, superior mechanical properties, and comparatively lower RS. Sun et al. [55] investigated that S-pattern exhibits the most favourable outcomes in terms of the minimum values of equivalent RS and maximum principal RS when compared to other patterns like that zig-zag, raster, alternate line, Hilbert, in-out spiral, and out-in spiral (Fig. 7). The S-pattern deposition is regarded as the most optimal among the six available patterns for deposition and shows excellent potential for MAM. The RS exhibited by the AlSi10Mg sample was comparatively lower when deposited using the parallel between layer (where the movements of the printing or laser beam are oriented in a

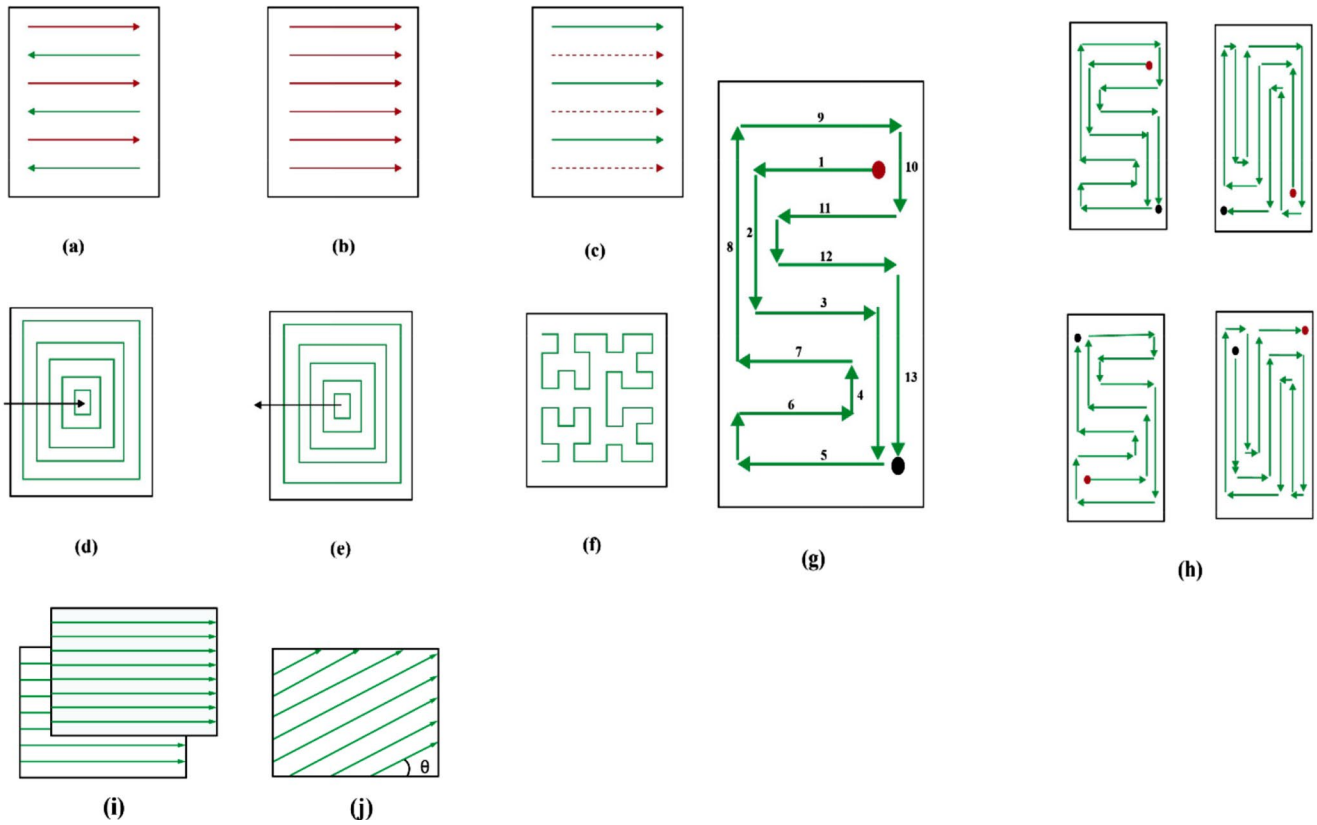

Fig. 7 Infill strategy: (**a**) zig-zag; (**b**) raster; (**c**) alternate-line; (**d**) out-in spiral; (**e**) in-out spiral; (**f**) Hilbert; (**g**) S-pattern one layer; (**h**) S-pattern multi-layer; (**i**) parallel between layer; (**j**) rotate within the layer

way that is parallel to the plane of the current layer being built) scanning strategy as opposed to the rotate within the layering (where the orientation of the scanning or printing path changes within a single layer of the 3D printed object) approach shown in Fig. 7 [56].

It should be noted that the impacts, as mentioned above, exhibit dissimilarities when considering singular versus multiple layers (specifically, RS in-plane anisotropy), as well as the direction of construction (which results in variations in strain/stress) [57]. When the energy density is too low, the material may not fuse properly, leading to weak inter-layer bonding and RS in part. On the other hand, when the energy density is too high, the material may become overheated, leading to excessive RS and distortion. In general, higher energy densities tend to result in higher RS in MAM parts. Higher energy densities can lead to more significant thermal gradients and faster cooling rates, which can cause differential cooling and solidification across the part, leading to RS [58–61].

The layer thickness in additive manufacturing can significantly affect the RS of the manufactured parts. In general, thinner layers tend to produce less RS than thicker layers. This is because thicker layers require more material to be deposited at once, which can lead to more thermal energy being applied to the part. This can cause the material to cool at a different rate, leading to RS within the part. Thinner layers, on the other hand, allow for more gradual cooling and can help to reduce the likelihood of thermal gradients forming in part.

The thinner layers may allow for more uniform heating and cooling of the part, which can further reduce RS [48, 58, 59, 62–64]. The RS in a MAM part can be significantly influenced by the geometry of the component and the utilization of support structures. The part's geometry has the potential to impact the cooling rate and the extent of thermal expansion and contraction, ultimately resulting in RS. The RS in a tall and slender structure may be more significant than a short and stubby structure owing to the higher temperature gradients and cooling rates experienced by the former. Utilizing auxiliary structures can also affect the remaining stresses in additive manufacturing components. Using support structures is a common practice in fabrication processes to secure the part and mitigate any potential distortion or bending. Incorporating supplementary structures may generate concentrated stress and thermal entrapment regions, resulting in further RS [58, 65].

Various methods can be employed to alleviate RS in MAM components. The utilization of optimized printing

parameters, such as laser power, layer height, energy density, scan strategy and speed, can aid in the reduction of the cooling rate and mitigate RS. Furthermore, implementing in-processing and post-processing methodologies detailed in Sect. 5, such as heat treatment or shot peening, can alleviate RS and enhance the mechanical characteristics of the component.

Residual stress impact on mechanical properties

The mechanical properties, microstructure, corrosion resistance, fracture initiation and propagation of MAM components are substantially influenced by RS [66, 67]. Tensile RS can reduce the load-carrying capacity of a material and can lead to premature failure due to cracking or fracture. In some cases, RS can enhance the strength of fabricated parts. The compressive RS can improve the fatigue life of build parts by reducing the propagation of cracks and the resistance of a material to bending or buckling. When a material is subjected to RS, it can create areas of localized strain that can alter the microstructure of the build parts, creating regions that are more susceptible to corrosion.

The RS can lead to the formation of microcracks and other defects in the MAM, which can provide sites for corrosion and crack, initiation, and propagation. In some cases, RS may indirectly influence the susceptibility of a fabricated parts to chemical reactions or corrosion. The presence of tensile RS can enhance the probability of stress corrosion cracking when subjected to corrosive environments. Even so, the predominant factor influencing alterations in chemical composition is the exposure to distinct chemical agents or circumstances, as opposed to the mere existence of RS [68]. Regarding fracture initiation, RS can create areas of high-stress concentration within the printed sample, increasing the likelihood of crack formation. These areas of high-stress concentration can be caused by residual tensile stresses or by changes in the microstructure of the material due to RS. Further, it can affect the rate at which cracks propagate through the material during fracture propagation. Residual tensile stresses can reduce the load-carrying capacity of the printed material, making it more susceptible to crack propagation.

The RS can contribute to the formation of intergranular cracks, particularly in materials that are susceptible to stress corrosion cracking [69]. RS can cause changes in the microstructure of printed material, particularly in areas where the stress is concentrated. The residual tensile stresses can cause elongation of the material's grains, while residual compressive stresses can cause compression of the grains. These changes in the microstructure can affect the material's mechanical properties, such as its strength, flexibility, and toughness. In addition to changes in the grain structure, RS can also cause changes in the chemical composition of the material. It can cause segregation of alloying elements, leading to changes in the material's corrosion resistance. RS can also cause changes in the concentration of defects and impurities within the MAM, which can affect its mechanical properties [70, 71].

The presence of RS may not necessarily have a detrimental effect on the material's performance. Shot peening is a surface treatment technique aimed at enhancing the fatigue behaviour of a material specimen through the induction of residual compressive stress [72]. RS is considered a crucial factor that influences the future implementation of MAM technology. This is due to its substantial effect on the deterioration of MAM product quality and the possible risk to product performance.

Residual stress analysis

This section has explored the defect incorporated due to RS in MAM process and developed a numerical model for the prediction of RS. The numerical model has developed to enable the incorporation of current developments into the existing body of research. The section not only consolidates current literature but also illustrates how emergent results add to the continuing discussion in the field. This approach enriches the review by providing a more comprehensive perspective and highlighting the relevance and impact of the proposed research in addressing existing gaps or advancing the field.

Defect incorporated into residual stress

The process of MAM continues to encounter obstacles in maintaining optimal product quality control. One such challenge is the occurrence of part distortion in terms of cracking, delamination, wrapping, and part deformation, as depicted in Figs. 8 and 9. These issues are attributed to the presence of RS [73, 74].

According to the evaluations' findings, most parts constructed through MAM displayed a consistent distortion pattern, whereby the farthest edges of the part were distorted in the direction of the build [9, 81–85]. Figure 9a and b demonstrate that the prism specimens constructed by selective laser melting (SLM) exhibited comparable distortion patterns in both the horizontal and vertical orientations, wherein the remote ends of the specimens peeled upwards along the build direction. Figure 9c and d indicate that the corners of the substrate exhibited the highest degree of wrapping following the deposition of six blocks via electron

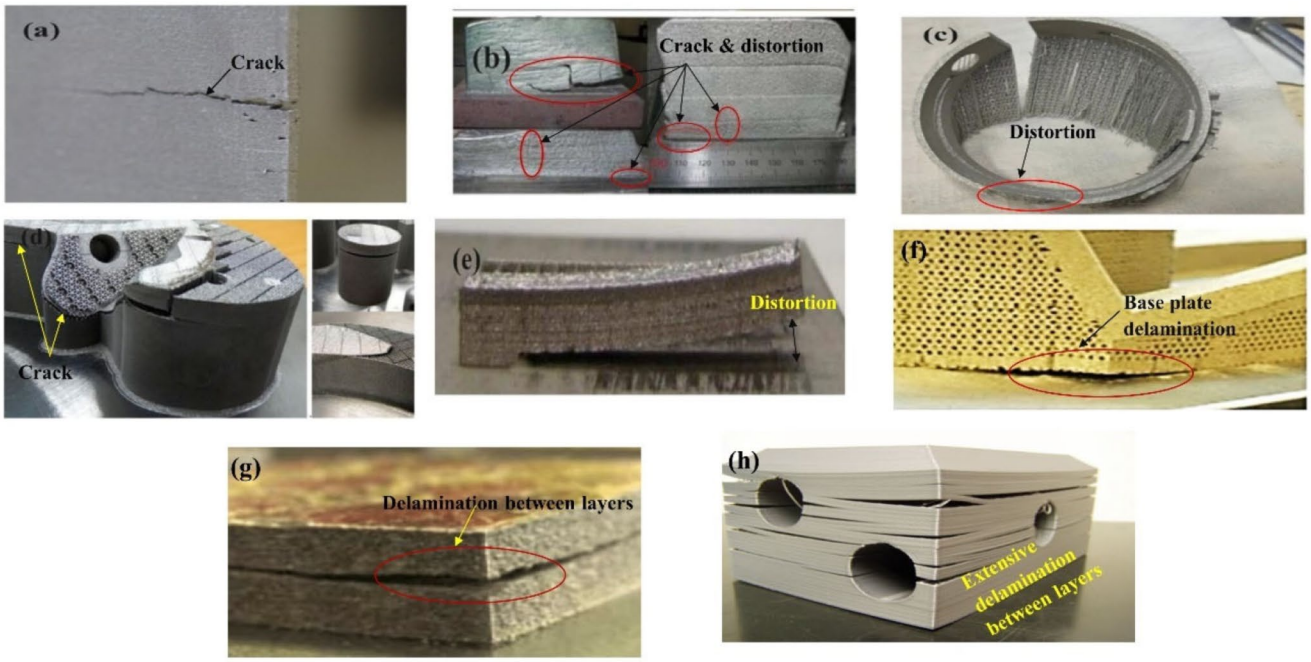

Fig. 8 Defects in MAM parts caused by RS: (**a**)-(**d**) Cracking [75–77]; (**e**) Distortion [78, 79]; (**f**) Base plate delamination [28]; (**g**), (**h**) Delamination between layers [80]. Reproduced with permission from Elsevier

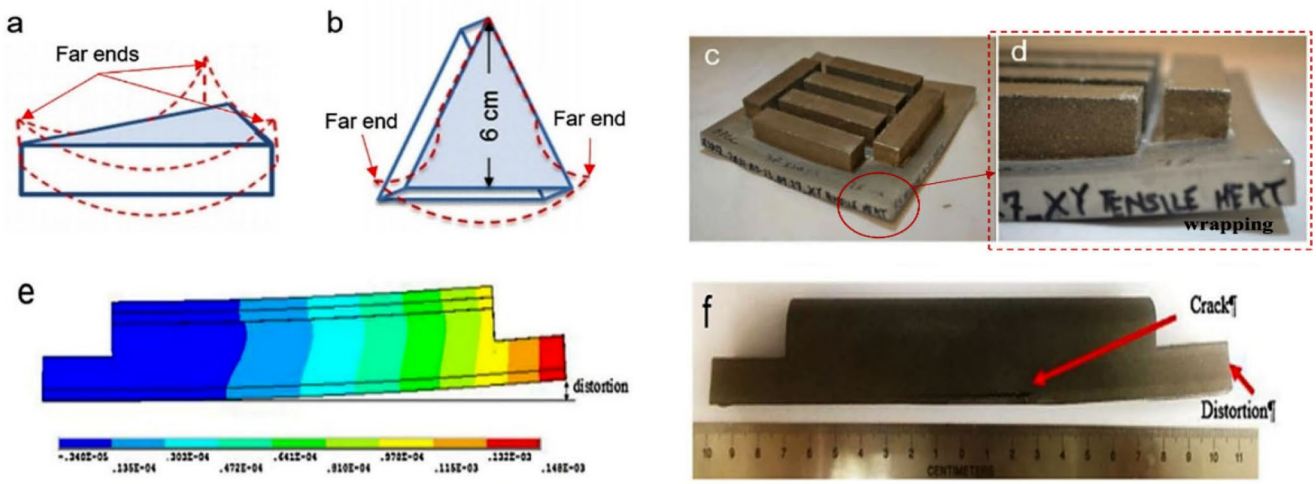

Fig. 9 Defect incorporated to metal additive manufactured parts: (**a**, **b**) Distortion in vertical and horizontal orientation [86]; (**c**, **d**) Wrapping in specimens [83]; (**e**, **f**) FEM-based distortion model with experimental validation [84]. Reproduced with permission from Elsevier

beam selective melting (EBSM). Figure 9e and f demonstrate that the occurrence of thermal stress during laser melting deposition (LMD) can result in the simultaneous generation of cracks and distortion.

The MAM process involves the quick heating of the material to its melting point, followed by rapid cooling and solidification at an exceptionally high cooling rate. The material is subjected to multiple cycles of the deposition process. Consequently, the MAM process is accompanied by an imbalance in thermo-mechanical-metallurgical factors. This disparity leads to a significant level of RS in the produced components, as evidenced by previous studies [86, 87]. Various methods for measuring part distortion are available, such as the coordinate measuring machine (CMM) [88, 89], laser displacement sensor (LDS) [74, 90–93], and digital image correlation (DIC) [9, 94].

Prediction model for distortion in MAM

The primary objective of this research is to calibrate a sequential thermo-mechanical FEA model for accurately predicting the inconsistent shrinkage behaviour of

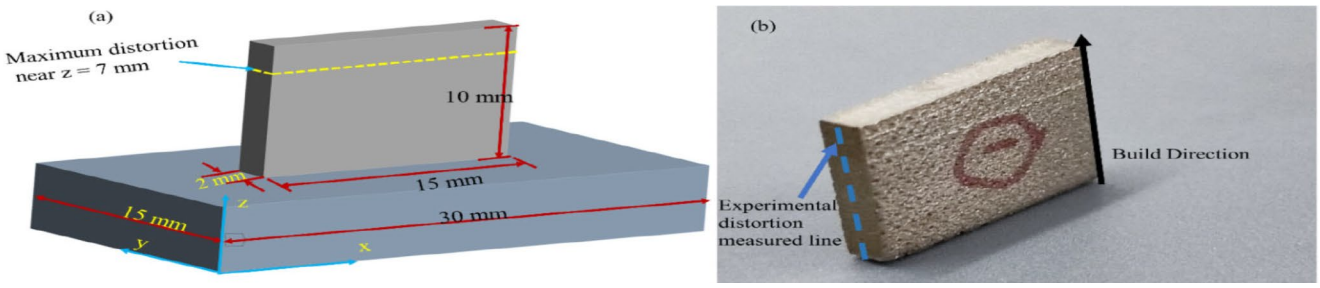

Fig. 10 (**a**) Rectangular block dimension; (**b**) L-PBF fabricated parts

Table 2 Ti64 processing parameters

Parameters	Value	Parameters	Value
Inert gas	Argon	Layer thickness (mm)	0.06
Beam diameter (mm)	0.065	Preheat temperature (°C)	200
Laser power (W)	500	Printing speed (mm/sec)	1250
Hatch distance (mm)	0.12	Energy density (J/mm3)	61

rectangular blocks manufactured by the laser powder bed fusion (L-PBF) process. ANSYS software was used for RS analysis due to its extensive usage and validation in both industry and academic research.

A sequential thermo-mechanical FEA was performed using the L-PBF AM modeler plugin integrated into the ANSYS finite element solver. To get a comprehensive understanding of the additive manufacturing simulation capabilities in ANSYS, it is recommended that the reader consults the ANSYS 2023 user handbook [95]. The fundamental measurements of the rectangular block under examination are shown in Fig. 10a. The dimensions of the block were as follows: it had a length of 15 mm, a width of 10 mm, and a thickness of 2 mm. The experimental and model setups were identical, with the rectangular block positioned centrally on the build plate as depicted in Fig. 10a. The build plate, often referred to as the base plate, has dimensions of 30 mm x 15 mm x 5 mm. The calibration component was manufactured via a L-PBF technique as illustrated in Fig. 10b, with the machine's process parameters configured as shown in the subsequent Table 2. Certain processing parameters were used as inputs in the simulation. The component was fabricated using Ti-6Al-4 V material, directly deposited onto a build plate without the use of any auxiliary support structures. After the fabrication process, a produced rectangular block was scanned using an ATOS Triple Scan (Capture 3D, Inc., Santa Ana, United States), which had a volumetric accuracy of 8 µm.

The Cartesian mesh was used to discretize the block, with an average element size of e = 0.5 mm, in order to strike a balance between precision and computing efficiency as shown in Fig. 11a. Conversely, the mesh size of the build plate was increased to a maximum element size of e = 1 mm. The construction of the block took place inside the yz-plane. The heat transfer study and subsequent structural analysis used an identical mesh.

The material Ti64 was designated for both base plate and rectangular block. The temperature-dependent physical and mechanical characteristics of Ti-6Al-4 V were included into the study using the data from the material database [96] (Fig. 12). The inelastic behaviour was characterized by a temperature independent plasticity model using bilinear-isotropic strain hardening behaviour, with a yield strength of σ_y = 1098 MPa and a tangent modulus of E_T = 1.332 GPa. Temperature-independent plasticity is a widely used technique in the modeling of part-scale L-PBF processes simulation [97–99]. The bilinear isotropic hardening material properties were applied to the model and triggered nonlinear effects for both the rectangular block and the base plate. The machine parameters were adjusted to maintain the deposition thickness at 0.06 mm, the hatching spacing at 0.12 mm and the laser speed at 1250 mm/sec.

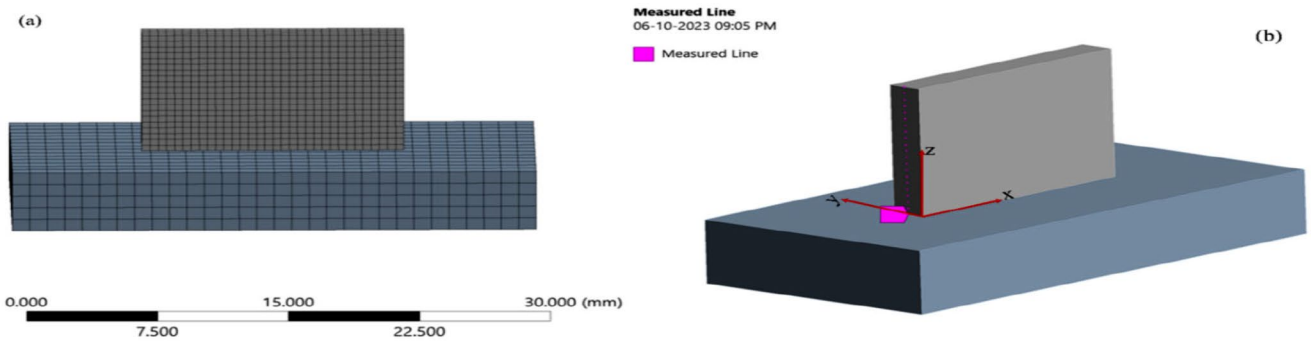

Fig. 11 (**a**) Model assembly highlighting the mesh to the model and build plate; (**b**) reference line of nodes

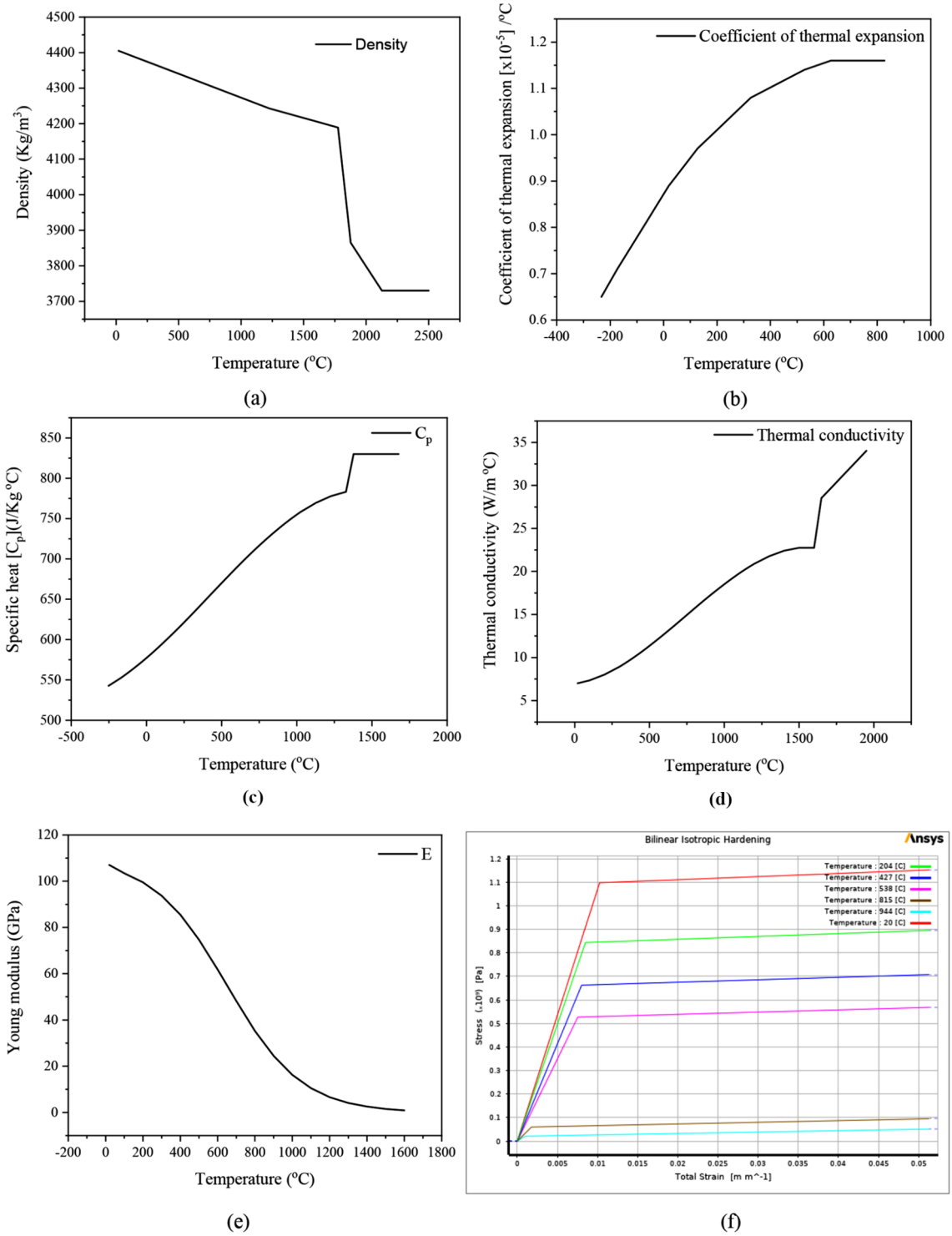

Fig. 12 Temperature-dependent material properties and plasticity: (**a**) Density, (**b**) coefficient of thermal expansion, (**c**) specific heat at constant pressure, (**d**) thermal conductivity, (**e**) elastic modulus and (**f**) plasticity behaviour

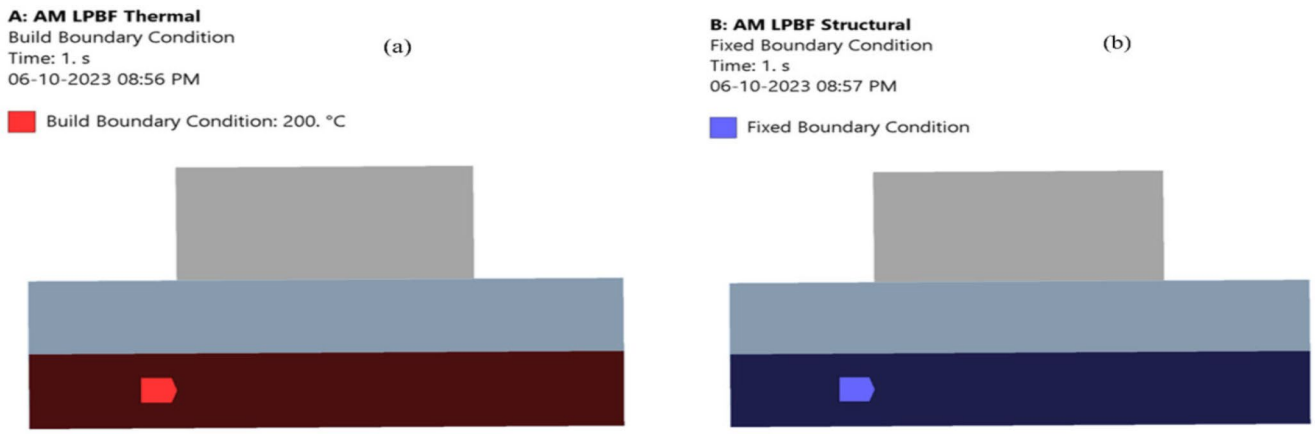

Fig. 13 Model subjected to thermo-mechanical boundary condition (**a**) build boundary condition; (**b**) fixed boundary condition

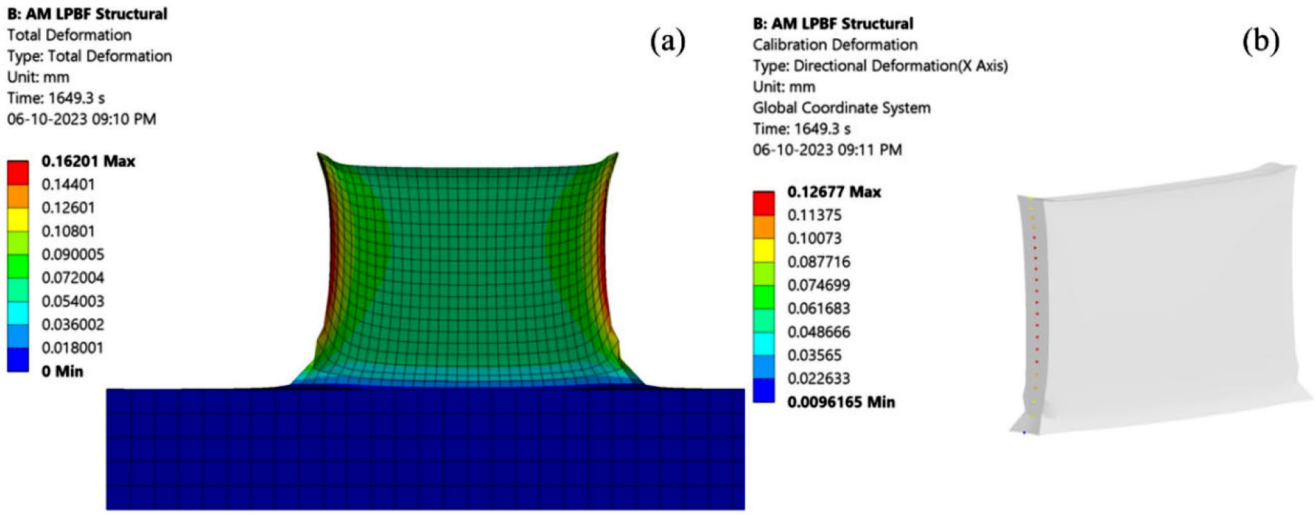

Fig. 14 FEA simulated results for (**a**) total deformation; (**b**) calibrated deformation

The preheating temperature of Ti-6Al-4 V powder and surrounding gas (argon) were considered as 200°C. The convection from the fabricated part to the build volume gas was included and the radiation was ignored during the fabrication. The gas convection coefficient was considered to 1×10^{-5} W/mm^2 °C. The convection from the fabricated part to the build volume powder was also included. The powder temperature was set to 200°C and the powder convection coefficient was set as 1×10^{-5} W/mm^2 °C. The cooldown temperature of the fabricated parts was considered as 22°C (room temperature). On the build plate, the thermal boundary condition and structural boundary condition were applied. The boundary conditions included a consistent preheat temperature during the building process, an ambient cooling temperature during the cooldown phase, and a fixed condition throughout the simulation. A fixed support was applied at the bottom face of the build plate, with a build boundary temperature of 200°C as shown in Fig. 13.

The transient temperature evaluation of the rectangular block during the L-PBF process was determined in the heat transfer analysis. The mechanical response and development of residual strains were determined based on the provided thermal history. The distortion of the L-PBF block was derived in the structural analysis. The block under investigation was anticipated to display significant distortion at the line of nodes located at X = 0 and Y = 1 mm along the Z-direction, as shown in Fig. 11b. A reference location was established for the purpose of calibrating the thermo-mechanical analysis and serving as a reference point for the final outcome. At the designated line of nodes, a target experimental distortion of 0.075 mm was assigned in the X-direction.

The Fig. 14 shows the result of FEA simulation for total deformation and calibrated deformation. The result revealed that the maximum total deformation and calibrated deformation value were determined to be 0.16201 mm and 0.12667 mm respectively at a default thermal strain scaling

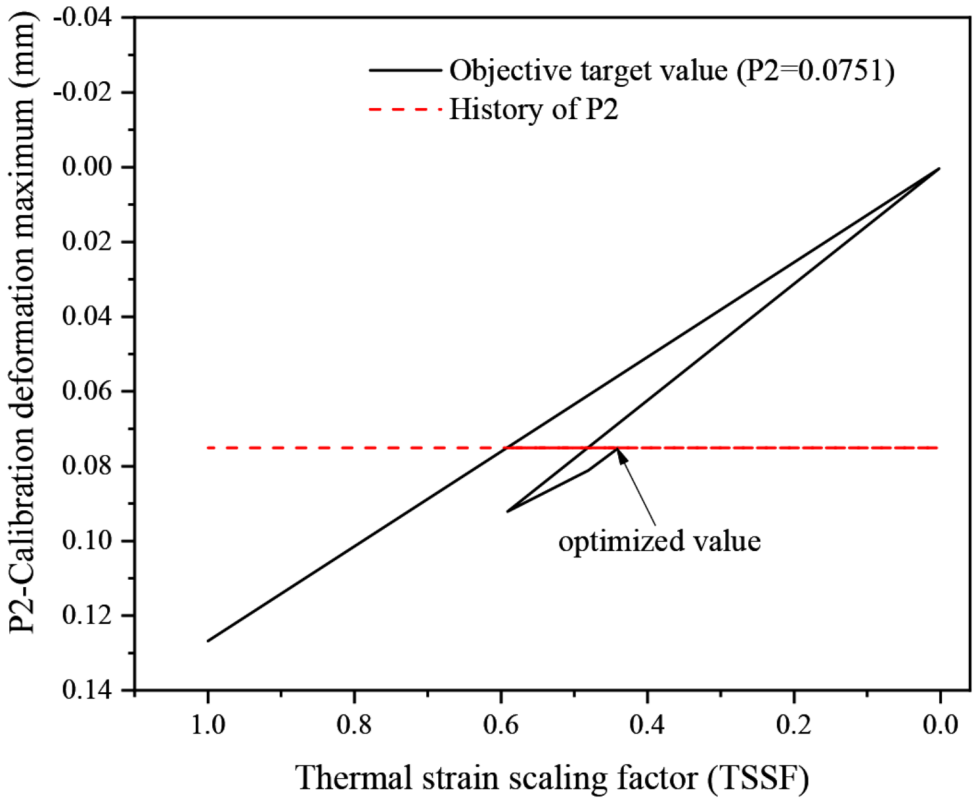

Fig. 15 Plot for optimized TSSF to achieve target objective

factor (TSSF)1. Direct optimization system was used to optimize the calibration through identify the optimum TSSF value that would yield the highest distortion along the measured line, therefore closely aligning with the experimental distortion value. The optimization system performed the thermal-structural simulations in an iterative manner. This was achieved by systematically varying the TSSF values, beginning from the default value of 1. The optimized result revealed that the calibrated TSSF value was determined to be 0.44, leading to a distortion measurement of 0.075073 mm. This is within the acceptable range of 1% tolerance as shown in Fig. 15.

Impact of in-process and post-process techniques in residual stress mitigation

Stresses in MAM are more significant in the vertical direction than in the scanning direction by a factor of 1.5–2.5 [77, 100–102], possibly due to asymmetry caused by MAM processing and material characteristics. Strong tensile tensions are introduced at a depth of around 40 µm from the cut surface in processes that necessitate Electrical Discharge Machining (EDM) cutting (particularly in SLM and EBM) [1]. Compared to SLM, parts processed through Electron Beam Melting (EBM) exhibit significantly lower levels of RS. This is attributed to the cooling rate, approximately one order of magnitude lower in EBM. This is evident from the solidification features, such as the dendrite arm spacing, observed in both processes [103–105]. Due to the extensive pre-heating of the powder bed and the isolated vacuum chamber, the cooling rate in EBM is substantially lower. The heat takes longer to dissipate and fade away from the EBM component. Preheating the substrate also shows the critical role in RS mitigation in MAM process. The RS decreases on increasing the preheating temperature of substrate/baseplate for SLM and Direct energy deposition (DED) techniques as shown in Fig. 16 [106, 107]. However, in-process and post-processing methods can minimize, shift, or even eradicate RS shown in Table 3. Laser shock peening (LSP), ultrasonic, hammer, shot peening (SP), heat treatment, explosive treatment, machining, and annealing are the post-process techniques used to mitigate the RS [47, 108–110].

Conclusion and future perspectives

The impact of RS on MAM is a critical aspect that significantly influences the mechanical properties, dimensional stability and reliability of the produced parts. This paper summarizes and discusses the typical characteristics of RS in MAM. The mechanism for the formation of RS has been proposed, and its effects have been analysed. This study examines the techniques employed for measuring RS, its

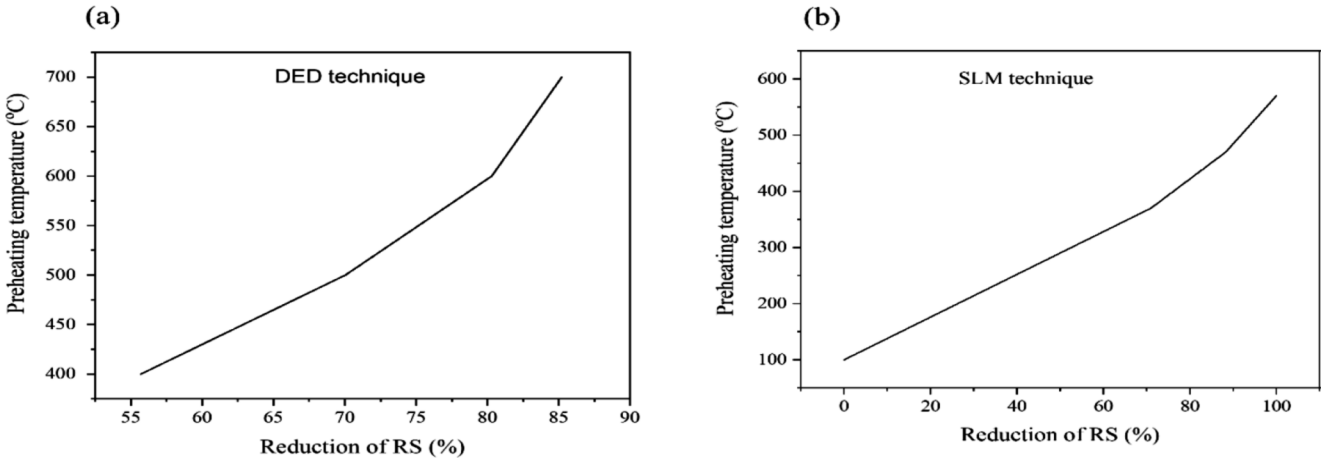

Fig. 16 Effect of RS on preheating temperature of substrate (**a**) 316 L stainless steel (**b**) Ti-6Al-4 V

correlation with microstructure, and the methods used to control them.

The generation of RS in MAM can be attributed to various formation mechanisms. Uneven plastic strain resulting from the temperature gradient, cool-down phase, and cooling rate gradient mechanisms are identified as critical contributors to RS formation. Heating and cooling rates influence the RS formation mechanism—parts processed through EBM exhibit significantly lower RS levels than SLM due to a lower cooling rate. The most commonly utilized RS measurement methods in MAM include HD, Ultrasonic wave, and XRD. These techniques are favoured due to their accessibility, the abundance of recognized standards such as ASTM and ISO, and ease of measurement. Process parameters significantly influence the formation of RS. To mitigate the impact of RS, one may consider implementing techniques such as the island and S-pattern scanning strategy, employing a thinner layer, reducing laser power, increasing scanning speed, and decreasing energy density. The parallel between the layer scanning strategy reduces the RS compared to the rotation within the layering technique. Scan trajectories can reduce about 55% RS.

It is strongly advised to utilize the pre-heating function of the equipment when conducting the MAM process with metal powder. Pre-heating the Ti64 powder over 570 °C reduces the RS [116]. The RS present in a tall and slender structure may be comparatively more significant than those in a short and stubby design.

Tensile RS has been observed to cause significant degradation in the mechanical characteristics of the fabricated parts. The presence of tensile RS in a material can negatively impact its load-carrying capacity, potentially resulting in early failure due to cracking or fracture. Compressive RS, on the other hand, can potentially prolong a material's fatigue life by decreasing the propagation of cracks. They also can make the material more resistant to buckling and bending. Distortion in damages, part deformation, wrapping, base plate and layers delamination, and dimensional inaccuracy incorporated to tensile RS in the fabricated parts. LSP, ultrasonic, hammer, SP, heat treatment, explosive treatment, and machining are the post-process techniques used to mitigate the RS. LSP reduces RS and induces work hardening, resulting in an increase in microhardness by 20%. Implementing post-heat treatment is a viable method for eliminating RS in a diverse range of materials. But it is essential to select the appropriate heat treatment regime. Heat treatment and machining combinedly improve 22% compressive RS on the surface. They were subjecting the base plate to a temperature of 200 °C resulted in a 40% reduction in RS aluminium alloy. In contrast, a temperature of approximately 570 °C yields minimal RS for titanium alloy. The annealing heat treatment process decreases RS by up to 70%. Hot isostatic pressing (HIP) reduces porosity ($<0.01\%$) and releases tensile RS but increases surface roughness.

The sequential thermo-mechanical modeling technique enhances the ability of accurately predicting the quality and performance of a product, providing useful information for optimizing the AM process. The model demonstrates its effectiveness as a resilient technique for minimizing RS and enhancing the overall reliability of AM. Additional investigation and improvement of this model might boost its precision and suitability for a wider variety of materials and geometries in AM. Numerous studies have been conducted in the field of process research, including both experimental and predictive model research. These investigations aim to ascertain the impact of various factors on RS or deformation of components produced using MAM techniques. The findings of these studies serve as valuable guidance in formulating and refining the MAM process. This process is both labour-intensive and costly. Hence, the incorporation of supplementary measurement information feedback and

Table 3 The significant impact of in-process and post-process techniques on RS modification

Materials	Measurement methods	RS modification technique	Findings
Aluminium alloy AA2198, NiTi	Hole drilling, XRD	LSP (In-process)	Mitigating the impact of thermal stress. Increased laser power results in the formation of non-equi-biaxial RS and decreased laser power results in the production of equi-biaxial RS. A smaller laser focus results in increased compressive RS at the surface [111]. Refine the microstructure with homogeneous material properties and compressive stress and improve the material properties [112, 113]. LSP and SP transform RS in MAM from tensile to compressive [114]. LSP induces work hardening resulting enhance in microhardness by 20%. The influence of LSP on the extent of diffusion has been seen to extend significantly to a depth of 0.6–0.7 mm below the surface shown in Fig. 17 [115].
Ti6Al4V	Hole drilling	Powder pre-heating (In-process)	Compressive stresses and the elimination of RS may result from pre-heating the powder to temperatures over 570 °C [116].
AlSi10Mg, Ti6Al4V, 304 stainless steel	Hole drilling, contour	Base plate heating (In-process)	Heated at 200 °C, 40% reduction of RS. RS reduces because of a lower thermal gradient [117]. At a temperature of 250 °C, no distortions occur [118]. The reduction in RS was found to be around 570 °C [116]. Compressive RS observed at a pre-heating temperature of 570–770 °C [119]. Arc pre-heating techniques reduce the RS in MAM [120].
Ti6Al4V, steel, aluminium alloy 2319, AA2319, S335JR steel, Ti-6Al-4 V	Contour, Neutron diffraction, FEM	Rolling (In-process)	During fabrication, high pressure of each layer reduces tensile RS than the unrolled specimen. The rolled specimens exhibited Compressive RS zones that were 150 and 250 MPa greater in magnitude compared to the unrolled specimens [121]. RS reduces, tensile strength and mechanical properties improve [122]. RS and distortion eliminate by side rolling and vertical rolling. The application of rolling the sample subsequent to every fourth layer yielded a similar impact on the distortion as the act of rolling after each individual layer [123]. The utilization of slotted roller has been found to be more efficacious in eliminating distortion when compared to profiled roller [124]. The application of a rolling load results in an increase in the depth of compressive RS. However, it has been observed that the rolling profile radius does not significantly affect the compressive RS [125].
Chrome molybdenum steel, Inconel 718, iron-based powder	Deep hole drilling, FEM	Scanning strategy (In-process)	Scan trajectories promote a 55% relief on RS [51]. The chessboard pattern ('island' shown in Fig. 6) scanning strategy reduces RS. The ideal island size was determined to be five mm^2 in size. Islands with dimensions of 5×5 mm^2 have superior mechanical properties and comparatively lower RS [126]. RS in the scanning direction is more tensile [121]. S-pattern exhibits minimum values of equivalent RS and maximum principal RS [55].
Inconel 718, Ti-6Al-4 V, Nickel aluminium bronze alloy	Neutron diffraction	Heat treatment (Post process)	Homogenize the microstructure [127]. RS reduced up to 70% at a temperature range of 600–700 °C [127]. Heat treatment is significant for stress relief, stabilizing the microstructure, and improving mechanical properties [128]. The application of quenching and tempering heat treatment results in the elimination of anisotropy in the MAM component [126]. The microstructure becomes homogeneous with stress relief [130]. Heat treatment reduces the tensile RS in MAM but cannot eliminate porosity [114]. Hot isostatic pressing (HIP) reduces porosity ($< 0.01\%$) and releases tensile RS but increases surface roughness [131].
Ti6Al4V, Chrome molybdenum steel	Hole drilling	Annealing (Post process)	Stresses redistribution and microstructure homogenization [116]. Tailored mechanical properties [116]. RS of additive manufacturing parts could potentially decrease up to 70% [51].
Steel	Hole drilling	Grinding and hard turning (Post process)	Compressive RS generated on both the machined subsurface and surface [132, 133].
Al7050-T7451	XRD	Cutting speed and feed rate (post-process)	Greater cutting rates produce thinner RS layers. Feed rate showed fewer variations in RS [134].
Ti6Al4V	XRD	Heat treatment + machining (post-process)	There was a notable rise of 22% in the compressive RS on the surface [135].
316 L steel	XRD	Magnetic field (Post-process)	The reduction of RS can be achieved by implementing motion control of the magnetic tool [136].

Table 3 (continued)

Materials	Measurement methods	RS modification technique	Findings
316 L steel, Ti6Al4V	XRD	Surface mechanical attrition treatment (SMAT) (Post-process)	Compressive RS was created in the range of 170 to 280 MPa [137]. In comparison to LSP, SMAT produces a more profound compressive RS zone [138].
Structural steel	Synchrotron XRD	Ultrasonic waves (Post-process)	Ultrasonic waves modify RS in depths up to 16 mm [139].

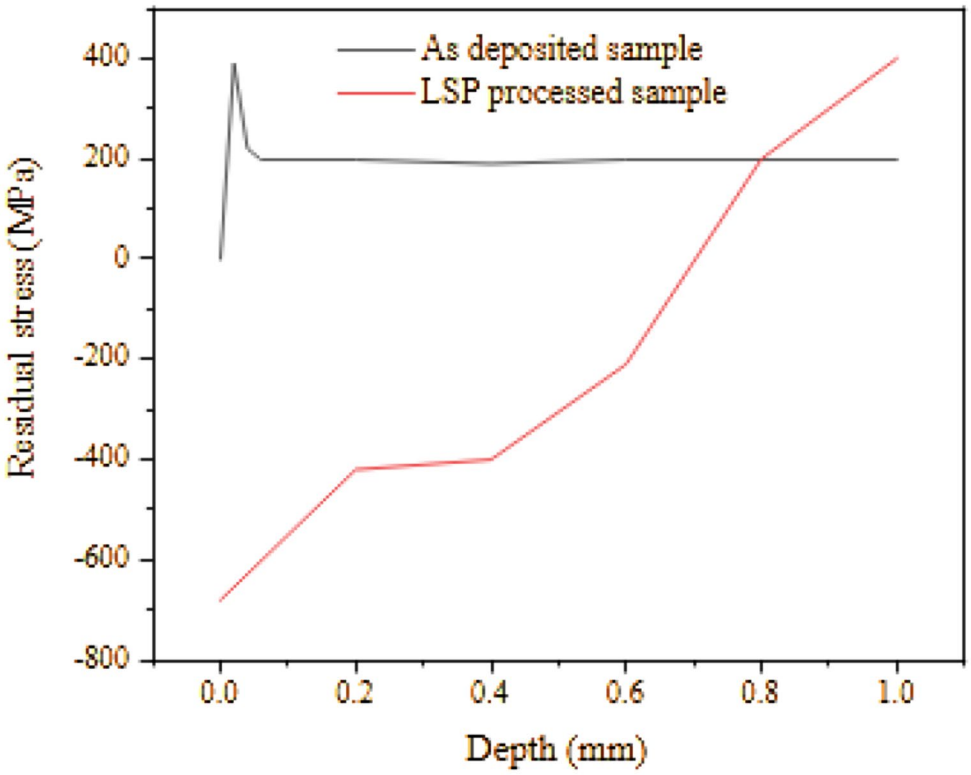

Fig. 17 Effect of LSP technique on RS generation in the Ni-Ti sample

process modification techniques into a closed loop system becomes very advantageous in reducing the possibility of modeling failure resulting from RS. An analysis may be conducted to examine the impact of geometric parameters of the additively manufactured components on the RS.

A specific set of NDT standards for MAM components should be devised. Given the complexity of MAM, this will increase our understanding of how to perform NDT on MAM components with high levels of accuracy and repeatability. More research has been conducted for selecting appropriate heat treatment regimes during the heat treatment process of building parts.

Acknowledgements The authors thank to Mr. Mohammad Akhtar (Mechanical Engineering Department), Al-Kabir Polytechnic Jamshedpur and Mr. Swaroop Kumar Mandal, NIT Jamshedpur, for their assistance and support, which enhanced the quality of the manuscript.

Competing interest None.

References

1. Mercelis P, Kruth JP (2006) Residual stresses in selective laser sintering and selective laser melting. Rapid Prototyp J 12(5):254–265. https://doi.org/10.1108/13552540610707013.
2. Brinksmeier E, Cammett JT, Konig W, Leskovar P, Peters J, Tonshoff HK (1982) Residual stresses-measurement and causes in machining processes. Ann CIRP 31(2):491–510. https://doi.org/10.1016/S0007-8506(07)60172-3.
3. Rossini NS, Dassisti M, Benyounis KY, Olabi AG (2012) Methods of measuring residual stresses in components. Mater Des 35:572–588. https://doi.org/10.1016/j.matdes.2011.08.022.
4. Kruth JP, Froyen L, Van Vaerenbergh J, Mercelis P, Rombouts M, Lauwers B (2004) Selective laser melting of iron-based powder. J Mater Process Technol 149(1–3):616–622. https://doi.org/10.1016/j.jmatprotec.2003.11.051.
5. Kruth JP, Deckers J, Yasa E, Wauthle R (2012) Assessing and comparing influencing factors of residual stresses in selective laser melting using a novel analysis method. Proc Inst Mech Eng B J Eng Manuf 226(6):1–12. https://doi.org/10.1177/0954405412437085.
6. Zyl I, Yadroitsava I, Yadroitsev I (2016) Residual stress in Ti6Al4V objects produced by direct metal laser sintering. South

Afr J Ind Eng 27(4):134–141. https://hdl.handle.net/10520/EJC199638
7. Norton JH, Rosenthal D (1944) Stress measurement by x-ray diffraction. Proc Soc Exp Stress Anal 1(2):73–76
8. Norton JH, Rosenthal D (1944) Application of the x-ray method of stress measurement to problems involving residual stress in metals. Proc Soc Exp Stress Anal 1(2):81–90
9. Wu AS, Brown DW, Kumar M, Gallegos GF, King WE (2014) An experimental investigation into additive manufacturing-induced residual stresses in 316L stainless steel. Metall Mater Trans A 45(13):6260–6270. https://doi.org/10.1007/s11661-014-2549-x
10. Chen M, Xing S, Liu H, Jiang C, Zhan K, Ji V (2020) Determination of surface mechanical property and residual stress stability for shot-peened SAF2507 duplex stainless steel by in situ X-ray diffraction stress analysis. J Mater Res Technol 9(4):7644–7654. https://doi.org/10.1016/j.jmrt.2020.05.028.
11. Zhang Z, Feng Y, Tan Q, Zou J, Li J, Zhou X, Wang Y (2019) Residual stress distribution in Ni-based superalloy turbine discs during fabrication evaluated by neutron/X-ray diffraction measurement and thermomechanical simulation. Mater Design 166:107603. https://doi.org/10.1016/j.matdes.2019.107603.
12. Swain D, Sharma A, Selvan SK, Thomas BP, Philip J (2019) Residual stress measurement on 3-D printed blocks of Ti-6Al-4V using incremental hole drilling technique. Procedia Struct Integr 14:337–344. https://doi.org/10.1016/j.prostr.2019.05.042.
13. Zhan Y, Liu C, Zhang J, Mo G, Liu C, 762 (2019) 138093. https://doi.org/10.1016/j.msea.2019.138093
14. Liu C, Lin C, Wang J, Wang J, Yan L, Luo Y, Yang M (2020) Residual stress distributions in thick specimens excavated from a large circular wire + arc additive manufacturing mockup. J Manuf Process 56:474–481. https://doi.org/10.1016/j.jmapro.2020.05.007.
15. De Oliveira AR, de Oliveira VF, Teixeira JC, Conte D, E. G (2021) Investigation of the build orientation effect on magnetic properties and Barkhausen noise of additively manufactured maraging steel 300. 38:101827. Additive Manufacturinghttps://doi.org/10.1016/j.addma.2020.101827.
16. Rizwee M, Kumar D, Kumar R (2024) Computational analysis of the Mechanical Compression of Additive Manufactured Lattice structures: a Numerical Study. Advances in Industrial Engineering in the industry 4.0 era. CRC, pp 147–156
17. Olabi AG, Hashmi MSJ (1996) Stress relief procedures for low carbon steel (1020) welded components. J Mater Process Technol 56:552–562. https://doi.org/10.1016/0924-0136(95)01869-7.
18. Kandil FA, Lord JD (2001) A review of residual stress measurement methods, a guide to technique selection. NPL Report MAT(A)04. http://eprintspublications.npl.co.uk/id/eprint/1873
19. Milbradt KP (1951) Ring-method determination of residual stresses. Proc SESA 9(1):63–74
20. Kiel S (1992) Experimental determination of residual stresses with the ring-core method and an online measuring system. Exp Tech 16(5):17–24. https://doi.org/10.1111/j.1747-1567.1992.tb00701.x
21. Kim S-H, Kim J-B, Lee W-J (2009) Numerical prediction and neutron diffraction measurement of the residual stresses for a modified 9Cr– 1Mo steel weld. J Mater Process Technol 209(8):3905–3913. https://doi.org/10.1016/j.jmatprotec.2008.09.012.
22. Paradowska A, Price JWH, Ibrahim R, Finlayson T (2005) A neutron diffraction of residual stress due to welding. J Mater Process Technol;164– 165:1099–1105. https://doi.org/10.1016/j.jmatprotec.2005.02.092.
23. Ajovalasit A, Petrucci G, Zuccarello B (1996) Determination of non-uniform residual stresses using the ring-core method. J Mater Process Technol 118(2):224–228. https://doi.org/10.1115/1.2804891.
24. Altpeter I, Dobmann G, Kröning M, Rabung M, Szielasko S (2009) Micro-magnetic evaluation of micro residual stresses of the IInd and IIIrd order. NDT&E Int 42:283–290. https://doi.org/10.1016/j.ndteint.2008.11.007.
25. Scholtes B (2007) Residual stress analysis of components with real geometries using the incremental hole-drilling technique and a differential evaluation method. Kassel university press GmbH
26. Vishay measurements group (2007) http://www.vishaypg.com/ (accessed March 1, 2011)
27. Lee HY, Nikbin KM, Dowd PO (2005) A generic approach for a linear fracture mechanics analysis of components containing residual stress. Int J Press Vess Pip 82:797–806. https://doi.org/10.1016/j.ijpvp.2005.05.001.
28. Acevedo R, Sedlak P, Kolman R, Fredel M (2020) Residual stress analysis of additive manufacturing of metallic parts using ultrasonic waves: state of the art review. J Mater Res Technol 9(4):9457–9477. https://doi.org/10.1016/j.jmrt.2020.05.092.
29. Liu J, Zhu H, Xu W (2011) Analysis of residual stresses in thick aluminum friction stir welded butt joints. Mater Des 32(4):2000–2005. https://doi.org/10.1016/j.matdes.2010.11.062.
30. Olabi AG, Hashmi MSJ (1995) The effect of post-weld heat treatment on mechanical properties and residual-stresses mapping in welded structural steel. J Mater Process Technol 55:117–122. https://doi.org/10.1016/0924-0136(95)01794-1.
31. Shadley JR, Rybicki EF, Shealy WS (1987) Application guidelines for the parting out in a through-thickness residual stress measurement procedure. Strain 23:157–166. https://doi.org/10.1111/j.1475-1305.1987.tb00640.x.
32. Tebedge N, Alpsten G, Tall L (1973) Residual-stress measurement by the sectioning method. Exp Mech 13(2):88–96. https://doi.org/10.1007/BF02322389
33. Mazzolani FM (1995) Aluminum alloy structures. 2nd ed. E&FN Spon, An imprint of Chapman and Hal;, ISBN: 978-0419177708
34. Lagerqvist O, Olsson A (2001) Residual stresses in welded I-girders made of stainless steel and structural steel. In: Helsinki: Proceedings of the ninth nordic steel construction conference; pp. 737–744
35. Young B, Lui WM (2005) Behavior of Cold-formed high-strength stainless steel sections. J Struct Eng, ASCE;131(11):1738–45. https://doi.org/10.1061/(ASCE)0733-9445(2005)131:11(1738)
36. Olabi AG, Hashmi MSJ (1998) Effects of the stress-relief conditions on a martensite stainless-steel welded component. J Mater Process Technol 77:216–225. https://doi.org/10.1016/S0924-0136(97)00420-2.
37. Prime MB, Gonzales AR (2000) In: Proceedings of the sixth international conference on residual stresses. Oxford, UK: IOM Communications Ltd. pp. 617–24
38. Olabi AG, Casalino G, Benyounis KY, Rotondo A (2007) Minimisation of the residual stress in the heat affected zone by means of numerical methods. Mater Des 28:2295–2302. https://doi.org/10.1016/j.matdes.2006.08.005.
39. Benyounis KY, Olabi AG, Abboud JH (2007) Assessment and minimization of the residual stress in dissimilar laser welding. Appl Mech Mater;7– 8:139–144. https://doi.org/10.4028/www.scientific.net/AMM.7-8.139.
40. Leggatt RH, Smith DJ, Smith SD, Faure F (1996) Development and experimental validation of the deep hole method for residual stress measurement. J Strain Anal 31(3):177–186. https://doi.org/10.1243/03093247V313177.
41. DeWald AT, Hill MR (2003) Improved data reduction for the deep hole method of residual stress measurement. J Strain Anal 38(1):65–78. https://doi.org/10.1243/030932403762671908.
42. Flaman MT, Herring GA (1985) Comparison of four hole-producing techniques for the center-hole residual-stress measurement method. Exp Tech 9:30–32. https://doi.org/10.1111/j.1747-1567.1985.tb02036.x

43. Flaman MT, Herring GA (1986) Ultra-high-speed center-hole technique for difficult machining materials. Exp Tech 10:34–35. https://doi.org/10.1111/j.1747-1567.1986.tb01370.x.
44. Zhang B, Dembinski L, Coddet C (2013) The study of the laser parameters and environment variables effect on mechanical properties of high compact parts elaborated by selective laser melting 316L powder. Mater Sci Eng A 584:21–31. https://doi.org/10.1016/j.msea.2013.06.055.
45. Venturi F, Taylor R (2023) Additive Manufacturing in the context of repeatability and reliability. J Mater Eng Perform 1–21. https://doi.org/10.1007/s11665-023-07897-3
46. Bartlett JL, Li X (2019) An overview of residual stresses in metal powder bed fusion. Addit Manuf 27:131–149. https://doi.org/10.1016/j.addma.2019.02.020.
47. Rizwee M, Kumar D, Hussain MM (2024) Enhancing the tribological characteristics of the Biocompatible Ti-6Al-4V Alloy via Heat Treatment: an experimental analysis. Tribol Int 110052. https://doi.org/10.1016/j.triboint.2024.110052
48. He B, Bi C, Li X, Wang W, Yang G (2023) Residual stresses and deformations of laser additive manufactured metal parts: a review. IntJ Mater Form 16(1):7. https://doi.org/10.1007/s12289-022-01729-w
49. Mukherjee T, Manvatkar V, De A, DebRoy T (2017) Mitigation of thermal distortion during additive manufacturing. Scr Mater 127:79–83. https://doi.org/10.1016/j.scriptamat.2016.09.001.
50. Hussein A, Hao L, Yan C, Everson R (2013) Finite element simulation of the temperature and stress fields in single layers built without support in selective laser melting. Mater Des (1980–2015). 52:638–647. https://doi.org/10.1016/j.matdes.2013.05.070.
51. Shiomi M, Osakada K, Nakamura K, Yamashita T, Abe F (2004) Residual stress within metallic model made by selective laser melting process. CIRP Ann Manuf Technol 53(1):195–198. https://doi.org/10.1016/S0007-8506(07)60677-5.
52. Loh L-E, Chua C-K, Yeong W-Y, Song J, Mapar M, Sing S-L et al (2015) Numerical investigation and an effective modeling on the selective laser melting (SLM) process with aluminium alloy 6061. Int J Heat Mass Transf 80:288–300. https://doi.org/10.1016/j.ijheatmasstransfer.2014.09.014.
53. Lu Y, Wu S, Gan Y, Huang T, Yang C, Junjie L, Lin J (2015) Study on the microstructure, mechanical property and residual stress of SLM inconel718 alloy manufactured by differing island scanning strategy. Opt Laser Technol. https://doi.org/10.1016/j.optlastec.2015.07.009. ;75197-206
54. Wu AS, Brown D, Kumar W, Gallegos M, King GF WE (2014) An experimental investigation into additive manufacturing-induced residual stresses in 316L stainless steel. Metall Mater Trans A 1–11. https://doi.org/10.1007/s11661-014-2549-x
55. Sun L, Ren X, He J, Zhang Z (2021) Numerical investigation of a novel pattern for reducing residual stress in metal additive manufacturing. J Mater Sci Technol 67:11–22. https://doi.org/10.1016/j.jmst.2020.05.080.
56. Wang L, Jiang X, Zhu Y, Zhu X, Sun J, Yan B (2018) An approach to predict the residual stress and distortion during the selective laser melting of AlSi10Mg parts. Int J Adv Manuf Technol 97:3535e46. https://doi.org/10.1007/s00170-018-2207-3
57. Withers PJ, Bhadeshia HK (2001) Residual stress overview. Part 2 nature and origins. Mater Sci Technol 17:366–375. https://doi.org/10.1179/026708301101510087
58. Jayanath S, Achuthan A (2018) A computationally efficient finite element framework to simulate additive manufacturing processes. J Manuf Sci Eng 140:041009. https://doi.org/10.1115/1.4039093.
59. Abusalma H, Eisazadeh H, Hejripour F, Bunn J, Aidun DK (2022) Parametric study of residual stress formation in Wire and Arc Additive Manufacturing. J Manuf Process 75:863–876. https://doi.org/10.1016/j.jmapro.2022.01.043.
60. Promoppatum P, Yao SC (2020) Influence of scanning length and energy input on residual stress reduction in metal additive manufacturing: Numerical and experimental studies. J Manuf Process 49:247–259. https://doi.org/10.1016/j.jmapro.2019.11.020.
61. Han Q, Gao J, Han C, Zhang G, Li Y (2021) Experimental investigation on improving the deposition rate of gas metal arc-based additive manufacturing by auxiliary wire feeding method. Weld World 65:35–45. https://doi.org/10.1007/s40194-020-00994-0
62. Li R, Xiong J, Lei Y (2019) Investigation on thermal stress evolution induced by wire and arc additive manufacturing for circular thin-walled parts. J Manuf Process 40:59–67. https://doi.org/10.1016/j.jmapro.2019.03.006.
63. Jinoop AN, Paul CP, Bindra KS (2019) Laser-assisted directed energy deposition of nickel super alloys: a review. *Proceedings of the Institution of Mechanical Engineers, Part L: Journal of Materials: Design and Applications*, *233*(11), 2376–2400. https://doi.org/10.1177/1464420719852658
64. Barath Kumar MD, Manikandan M (2022) Assessment of process, parameters, residual stress mitigation, post treatments and finite element analysis simulations of wire arc additive manufacturing technique. Met Mater Int 28(1):54–111. https://doi.org/10.1007/s12540-021-01015-5
65. Fan D, Gao M, Li C, Huang J, Yu X (2022) Residual stress and microstructure properties by trailing cooling of argon gas of wire and arc additive manufacturing. J Manuf Process 77:32–39. https://doi.org/10.1016/j.jmapro.2022.03.007.
66. Romano S, Bru¨ ckner-Foit A, Brando A, Gumpinger J, Ghidini T, Beretta S (2018) Fatigue properties of AlSi10Mg obtained by additive manufacturing: defect-based modelling and prediction of fatigue strength. Eng Fract Mech 187:165e89. https://doi.org/10.1016/j.engfracmech.2017.11.002.
67. Jing S, Zhang Y, Ke S (2016) The numerical simulation for effect of vibratory stress relief on titanium alloy Ti-6Al-4V fatigue life. https://doi.org/10.1007/978-981-10-2669-0_57. Springer Singapore
68. Prando D, Brenna A, Diamanti MV, Beretta S, Bolzoni F, Ormellese M, Pedeferri M (2017) Corrosion of titanium: part 1: aggressive environments and main forms of degradation. J Appl Biomater Funct Mater 15(4):e291–e302. https://doi.org/10.5301/jabfm.5000387
69. Zhang J, Song B, Cai C, Zhang L, Shi Y (2022) Tailorable microstructure and mechanical properties of selective laser melted TiB/Ti–6Al–4V composite by heat treatment. Adv Powder Mater 1(2):100010. https://doi.org/10.1016/j.apmate.2021.10.001.
70. Shi ZF, Guo HZ, Han JY, Yao ZK (2013) Microstructure and mechanical properties of TC21 titanium alloy after heat treatment. Trans Nonferrous Met Soc China 23(10):2882–2889. https://doi.org/10.1016/S1003-6326(13)62810-1.
71. Sui S, Chew Y, Hao Z, Weng F, Tan C, Du Z, Bi G (2022) Effect of cyclic heat treatment on microstructure and mechanical properties of laser aided additive manufacturing Ti–6Al–2Sn–4Zr–2Mo alloy. Adv Powder Mater 1(1):100002. https://doi.org/10.1016/j.apmate.2021.09.002.
72. Wang C, Jiang C, Fei C, Zhao Y, Zhu K, Chai Z (2016) Effect of shot peening on the residual stresses and microstructure of tungsten cemented carbide. Mater Des 95:159e64. https://doi.org/10.1016/j.matdes.2016.01.101
73. Paul R, Anand S, Gerner F (2014) Effect of thermal deformation on part errors in metal powder based additive manufacturing processes. J Manuf Sci Eng 136:31009. https://doi.org/10.1115/1.4026524.
74. Dunbar AJ, Denlinger ER, Heigel J, Michaleris P, Guerrier P, Martukanitz R et al (2016) Development of experimental method for in situ distortion and temperature measurements during the laser powder bed fusion additive manufacturing process. Additive Manuf 12:25–30. https://doi.org/10.1016/j.addma.2016.04.007.

75. Lai YB, Liu WJ, Zhao JB, Zhao YH, Wang FY, Han WC (2013) Experimental study on residual stress in titanium alloy laser additive manufacturing. Appl Mech Mater 431:20e6. https://doi.org/10.4028/www.scientific.net/AMM.431.20
76. Yadroitsev I, Yadroitsava I (2015) Evaluation of residual stress in stainless steel 316L and Ti6Al4V samples produced by selective laser melting. Virtual Phys Prototyp 10:67e76. https://doi.org/10.1080/17452759.2015.1026045.
77. Parry L, Ashcroft IA, Wildman RD (2016) Understanding the effect of laser scan strategy on residual stress in selective laser melting through thermo-mechanical simulation. Additive Manuf 12:1–15. https://doi.org/10.1016/j.addma.2016.05.014.
78. LN C. (2017) An experimental investigation of residual stress development during selective laser melting of Ti-6Al-4V. http://rave.ohiolink.edu/etdc/view?acc_num=wright1515112797193544
79. Chen Q, Liang X, Hayduke D, Liu J, Cheng L, Oskin J et al (2019) An inherent strain based multiscale modeling framework for simulating part-scale residual deformation for direct metal laser sintering. https://doi.org/10.1016/j.addma.2019.05.021. Additive Manufacturing; 28:406 – 18
80. DebRoy, T., Wei, H. L., Zuback, J. S., Mukherjee, T., Elmer, J. W., Milewski, J. O.,… Zhang, W. (2018). Additive manufacturing of metallic components–process, structure and properties. Progress in Materials Science. 2018; 92, 112–224. https://doi.org/10.1016/j.pmatsci.2017.10.001
81. Montevecchi F, Venturini G, Grossi N et al (2017) Finite element mesh coarsening for effective distortion prediction in wire arc additive manufacturing. Addit Manuf 18:145–155. https://doi.org/10.1016/j.addma.2017.10.010.
82. Xie D, Lv F, Zhao J et al (2021) Towards a comprehensive understanding of distortion in additive manufacturing based on assumption of constraining force. Virtual Phys Prototyp 16:85–97. https://doi.org/10.1080/17452759.2021.1881873
83. Prabhakar P, Sames W, Dehoff R et al (2015) Computational modeling of residual stress formation during the electron beam melting process for Inconel 718. Addit Manuf 7:83–91. https://doi.org/10.1016/j.addma.2015.03.003
84. Zhang Y, Zhang J (2017) Finite element simulation and experimental validation of dis- tortion and cracking failure phenomena in direct metal laser sintering fabricated component. Addit Manuf 16:49–57. https://doi.org/10.1016/j.addma.2017.05.002
85. Wen Y, Zhang B, Liu S et al (2020) A novel experimental method for in situ strain measurement during selective laser melting. Virtual Phys Prototyp 15(s1):83–95. https://doi.org/10.1080/17452759.2020.1842137.
86. Wu A, Brown S, Donald W et al (2014) An experimental investigation into additive man- ufacturing-induced residual stresses in 316L stainless steel. Metall Mater Trans A 45(13):6260–6270. https://doi.org/10.1007/s11661-014-2549-x
87. Xiao Z, Chen C, Zhu H, Hu Z, Nagarajan B, Guo L et al (2020) Study of residual stress in selective laser melting of Ti6Al4V. Mater Des 193:108846. https://doi.org/10.1016/j.matdes.2020.108846.
88. Marimuthu S, Clark D, Allen J et al (2012) Finite element modelling of substrate thermal distortion in direct laser additive manufacture of an aero-engine component. Proc Inst Mech Eng Part C J Mech Eng Sci 227(9):1987–1999. https://doi.org/10.1177/0954406212470363
89. Ghnatios C, Rai K, Hascoet N et al (2021) Reduced order modeling of selective laser melting: from calibration to parametric part distortion. Int J Mater Form 14:973–986. https://doi.org/10.1007/s12289-021-01613-z
90. Dunbar AJ, Denlinger ER, Gouge MF et al (2017) Comparisons of laser powder bed fusion additive manufacturing builds through experimental in situ distortion and temperature measurements. Addit Manuf 15:57–65. https://doi.org/10.1016/j.addma.2017.03.003.
91. Denlinger ER, Gouge M, Irwin J et al (2017) Thermomechanical model development and in situ experimental validation of the laser powder-bed fusion process. Addit Manuf 16:73–80. https://doi.org/10.1016/j.addma.2017.05.001.
92. Denlinger ER, Heigel JC, Michaleris P et al (2015) Effect of interlayer dwell time on distortion and residual stress in additive manufacturing of titanium and nickel alloys. J Mater Process Technol 215:123–131. https://doi.org/10.1016/j.jmatprotec.2014.07.030.
93. Denlinger ER, Heigel JC, Michaleris P (2015) Residual stress and distortion modeling of electron beam direct manufacturing Ti-6Al 4V. Proc Inst Mech Eng Part B J Eng Manuf 229(10):1803–1813. https://doi.org/10.1177/0954405414539494.
94. Biegler M, Graf B, Rethmeier M (2018) In-situ distortions in LMD additive manufacturing walls can be measured with digital image correlation and predicted using numerical simulations. Addit Manuf 20:101–110. https://doi.org/10.1016/j.addma.2017.12.007
95. ANSYS Inc (2023) ANSYS Additive user guidance 2023R2
96. Inc ANSYS (2021) Ansys additive suite. Technical Report, Canonsburg, Pennsylvania, United States
97. Yang Y, Allen M, London T, Oancea V (2019) Residual strain predictions for a powder bed fusion inconel 625 single cantilever part. Integrat Mater Manuf Innovat 8(3):294–304. https://doi.org/10.1007/s40192-019-00144-5
98. Minetola P, Stiuso V, Calignano F, Galati M, Khandpur MS, Fontana L (2021) Experimental validation of laser powder bed fusion simulation. IOP Conf Ser : Mater Sci Eng 1091(1):012048. https://doi.org/10.1088/1757-899x/
99. Alvarez P, Ecenarro J, Setien I, Sebastian MS, Echeverria A, L (2016) Eciolaza, computationally efficient distortion prediction in powder bed fusion additive manufacturing. Int J Eng Res Sci 2(10):39–46
100. Gusarov AV, Pavlov M, Smurov I (2011) Residual stresses at laser surface remelting and additive manufacturing. Phys Proc 12:248–254. https://doi.org/10.1016/j.phpro.2011.03.032.
101. Robinson J, Ashton I, Fox P, Jones E, Sutcliffe C (2018) Determination of the effect of scan strategy on residual stress in laser powder bed fusion additive manufacturing. Addit Manuf 23:13–24. https://doi.org/10.1016/j.addma.2018.07.001.
102. Yadroitsava I, Grewar S, Hattingh D, Yadroitsev I (2015) Residual stress in SLM Ti6Al4V alloy specimens. Mater Sci Forum 828–829:305–310. https://doi.org/10.4028/www.scientific.net/MSF.828-829.305
103. Amato K, Hernandez J, Murr L, Martinez E, Gaytan S, Shindo P, Collins S (2012) Comparison of microstructures and properties for a Ni-base superalloy (alloy 625) fabricated by electron beam melting. J Mater Sci Res 1(2):3. https://doi.org/10.5539/jmsr.v1n2p3.
104. Vrancken B, Thijs L, Kruth J, Van Humbeeck J (2012) Heat treatment of Ti6Al4V produced by selective laser melting: microstructure and mechanical properties. J Alloys Compd 541(0):177–185. https://doi.org/10.1016/j.jallcom.2012.07.022.
105. Li C, Guo YB, Zhao JB (2017) Interfacial phenomena and characteristics between the deposited material and substrate in selective laser melting inconel 625. J Mater Process Technol. https://doi.org/10.1016/j.jmatprotec.2016.12.033. ;243269-281
106. Waqar S, Guo K, Sun J (2022) Evolution of residual stress behavior in selective laser melting (SLM) of 316L stainless steel through preheating and in-situ re-scanning techniques. Opt Laser Technol 149:107806. https://doi.org/10.1016/j.optlastec.2021.107806.
107. Lu X, Lin X, Chiumenti M, Cervera M, Hu Y, Ji X, Huang W (2019) Residual stress and distortion of rectangular and S-shaped Ti-6Al-4V parts by Directed Energy Deposition: Modelling and experimental calibration. Additive Manuf 26:166–179. https://doi.org/10.1016/j.addma.2019.02.001

108. Kudryavtsev Y, Kleiman J (2011) Residual stress management: measurement, fatigue analysis and beneficial redistribution. In: Conference Proceedings for the Society for Experimental Mechanics Series. pp. 119–29. https://doi.org/10.1007/978-1-4614-0225-1
109. Guz' AN, Makhort FG (2000) The physical fundamentals of the ultrasonic non-destructive stress analysis of solids. Int Appl Mech, Springer;36(9):1119–49. https://doi.org/10.1023/A:1009442132064
110. Newell DJ, O'Hara RP, Cobb GR, Palazotto AN, Kirka MM, Burggraf LW et al (2019) Mitigation of scan strategy effects and material anisotropy through supersolvus annealing in LPBF IN718. Mater Sci Eng A 764:138230. https://doi.org/10.1016/j.msea.2019.138230
111. Keller S, Chupakhin S, Staron P, Maawad E, Kashaev N, Klusemann B (2018) Experimental and numerical investigation of residual stresses in laser shock peened AA2198. J Mater Process Technol 255:294–307. https://doi.org/10.1016/j.jmatprotec.2017.11.023.
112. Sun R, Li L, Zhu Y, Guo W, Peng P, Cong B, Liu L (2018) Microstructure,residual stress and tensile properties control of wire-arc additive manufactured 2319 aluminum alloy with laser shock peening. J Alloys Compd 747:255–265. https://doi.org/10.1016/j.jallcom.2018.02.353
113. Varin S, Agarwal M, Chugh A, Manikandan M, Prabhakaran S, Kalainathan S, Arivazhagan N (2019) Effect of laser shock peening on commercially pure titanium-1 weldment fabricated by gas tungsten arc welding technique. Trans Indian Inst Met 72:1569–1573. https://doi.org/10.1007/s12666-019-01704-1
114. Ye C, Zhang C, Zhao J, Dong Y (2021) Effects of post-processing on the surface finish, porosity, residual stresses, and fatigue performance of additive manufactured metals: a review. J Mater Eng Perform 30:6407–6425. https://doi.org/10.1007/s11665-021-06021-7
115. Shiva S, Palani IA, Paul CP, Bindra KS (2021) Laser shock peening of Ni-Ti bulk structures developed by laser additive manufacturing. J Mater Eng Perform 30(8):5603–5613. https://doi.org/10.1007/s11665-021-05799-w
116. Ali H, Ma L, Ghadbeigi H, Mumtaz K (2017) In-situ residual stress reduction, martensitic decomposition and mechanical properties enhancement through high temperature powder bed pre-heating of selective laser melted Ti6Al4V. https://doi.org/10.1016/j.msea.2017.04.033. Mat Sci Eng-A;695211-220
117. Li C, Liu ZY, Fang XY, Guo YB (2018) Residual stress in metal additive manufacturing. In: 4th CIRP Conference on Surface Integrity. pp. 348–53. https://doi.org/10.1016/j.procir.2018.05.039
118. Buchbinder D, Meiners W, Pirch N, Wissenbach K, Schrage J (2014) Investigation on reducing distortion by pre-heating during manufacture of aluminum components using selective laser melting. J Laser Appl 26(1):012004. https://doi.org/10.2351/1.4828755.
119. Ali H, Ghadbeigi H, Hosseinzadeh F, Oliveira J, Mumtaz K (2019) Effect of pre-emptive in situ parameter modification on residual stress distributions within selective laser-melted Ti6Al4V components. Int J Adv Manuf Technol 103:4467–4479. https://doi.org/10.1007/s00170-019-03860-6
120. Liu H, Li Z, Li W, Zhang W, Wang T, Liu W (2022) Influence of Arc pre-heating on stress and strain of Additive Manufactured Components. J Mater Eng Perform 1–14. https://doi.org/10.1007/s11665-022-07565-y
121. Martina F, Roy MJ, Szost BA, Terzi S, Colegrove PA, Williams SW et al (2016) Residual stress of as-deposited and rolled wire+arc additive manufacturing Ti-6Al-4V components. Mater Sci Technol 32(14). https://doi.org/10.1080/02670836.2016.1142704.
122. Nemani AV, Ghaffari M, Nasiri A (2020) Comparison of microstructural characteristics and mechanical properties of shipbuilding steel plates fabricated by conventional rolling versus wire arc additive manufacturing. Additive Manuf 32:101086. https://doi.org/10.1016/j.addma.2020.101086.
123. Hönnige JR, Colegrove PA, Ganguly S, Eimer E, Kabra S, Williams S (2018) Control of residual stress and distortion in aluminium wire+arc additive manufacture with rolling. Additive Manuf 22:775–783. https://doi.org/10.1016/j.addma.2018.06.015.
124. Colegrove PA, Coules HE, Fairman J, Martina F, Kashoob T, Mamash H, Cozzolino LD (2013) Microstructure and residual stress improvement in wire and arc additively manufactured parts through high-pressure rolling. J Mater Process Technol 213(10):1782–1791. https://doi.org/10.1016/j.jmatprotec.2013.04.012
125. Abbaszadeh, M., Hönnige, J. R., Martina, F., Neto, L., Kashaev, N., Colegrove, P.,… Klusemann, B. (2019) Numerical investigation of the effect of rolling on the localized stress and strain induction for wire+arc additive manufactured structures. Journal of Materials Engineering and Performance; *28*, 4931–4942. https://doi.org/10.1007/s11665-019-04249-y
126. Lu Y, Wu S, Gan Y, Huang T, Yang C, Junjie L et al (2015) Study on the microstructure, mechanical property and residual stress of SLM inconel-718 alloy manufactured by differing island scanning strategy. Opt Laser Technol 75:197–206. https://doi.org/10.1016/j.optlastec.2015.07.009.
127. Aba-Perea PE, Pirling T, Preuss M (2016) In-situ residual stress analysis during annealing treatments using neutron diffraction in combination with a novel furnace design. Mater Des 110(15):925–931. https://doi.org/10.1016/j.matdes.2016.07.078.
128. Wang J, Lin X, Wang M, Li J, Wang C, Huang W (2020) Effects of subtransus heat treatments on microstructure features and mechanical properties of wire and arc additive manufactured Ti–6Al–4V alloy. Mater Sci Engineering: A 776:139020. https://doi.org/10.1016/j.msea.2020.139020.
129. Shen, C., Pan, Z., Ding, D., Yuan, L., Nie, N., Wang, Y., … Li, H. (2018) The influence of post-production heat treatment on the multi-directional properties of nickel-aluminum bronze alloy fabricated using wire-arc additive manufacturing process. Additive Manufacturing;23, 411–421. https://doi.org/10.1016/j.addma.2018.08.008
130. Wang X, Chou K (2019) The effects of stress relieving heat treatment on the microstructure and residual stress of Inconel 718 fabricated by laser metal powder bed fusion additive manufacturing process. J Manuf Process 48:154–163. https://doi.org/10.1016/j.jmapro.2019.10.027.
131. Ge J, Pillay S, Ning H (2023) Post-process treatments for additive-manufactured metallic structures: a Comprehensive Review. J Mater Eng Perform 1–50. https://doi.org/10.1007/s11665-023-08051-9
132. Matsumoto Y, Hashimoto F, Lahoti G (1999) Surface integrity generated by precision hard turning. CIRP Ann Manuf Technol 48(1):59–62. https://doi.org/10.1016/S0007-8506(07)63131-X.
133. Guo YB, Li W, Jawahir IS (2009) Surface integrity characterization and prediction in machining of hardened and difficult-to-machine alloys: a state-of-art research review and analysis. Mach Sci Technol 13:437–470. https://doi.org/10.1080/10910340903454922.
134. Tang ZT, Liu ZQ, Wan Y, Ai X (2008) Study on residual stresses in milling aluminum alloy 7050-T7451. Advanced design and manufacture to gain a competitive edge. Springer, pp 169–178. https://doi.org/10.1007/978-1-84800-241-8_18
135. Oyelola O, Crawforth P, Saoubi R, Clare AT (2017) On the machinability of directed energy deposited Ti6Al4V. https://doi.org/10.1016/j.addma.2017.11.005. Addit Manuf;245
136. Yamaguchi H, Fergani O, Wu PY (2017) Modification using magnetic field-assisted finishing of the surface roughness

and residual stress of additively manufactured components. https://doi.org/10.1016/j.cirp.2017.04.084. CIRP Ann Manuf Technol;1642

137. Portella Q, Chemkhi M, Retraint D (2018) Residual stresses in analysis in AISI 316L processed by selective laser melting (SLM) treated by mechanical post-processing treatments. Mater Res Proc 6:271–276 ECRS-10
138. Galitelli D, Retraint D, Rouhaud E (2014) Comparison between conventional shot peening (SP) and surface mechanical attrition treatment (SMAT) on a titanium alloy. Adv Mater Res 996:964–968. https://doi.org/10.4028/www.scientific.net/AMR.996.964
139. Gao H, Dutta RK, Huizenga RM, Amirthalingam M, Hermans MJM et al (2014) Stress relaxation due to ultrasonic impact treatment on multi-pass welds. Sci Technol Weld Join 19(6). https://doi.org/10.1179/1362171814Y.0000000219.